



## Kinetic and mechanistic study of bimetallic Pt-Pd/Al<sub>2</sub>O<sub>3</sub> catalysts for CO and C<sub>3</sub>H<sub>6</sub> oxidation

Melanie J. Hazlett<sup>a</sup>, Melanie Moses-Debusk<sup>b</sup>, James E. Parks II<sup>b</sup>, Lawrence F. Allard<sup>c</sup>, William S. Epling<sup>a,\*</sup>

<sup>a</sup> Department of Chemical and Biomolecular Engineering, University of Houston, Houston, TX 77204, United States

<sup>b</sup> Fuels, Engines, and Emissions Research Center, Oak Ridge National Laboratory, Knoxville, TN 37932, United States

<sup>c</sup> Materials Science and Technology Division, Oak Ridge National Laboratory, Oak Ridge, TN 37831, United States

### ARTICLE INFO

#### Article history:

Received 14 September 2016

Accepted 17 September 2016

Available online 21 September 2016

#### Keywords:

Oxidation catalyst

CO oxidation

Propylene oxidation

Bimetallic Pt:Pd catalysts

### ABSTRACT

Low temperature combustion (LTC) diesel engines are being developed to meet increased fuel economy demands. However, some LTC engines emit higher levels of CO and hydrocarbons and therefore diesel oxidation catalyst (DOC) efficiency will be critical. Here, CO and propylene oxidation were studied, as representative LTC exhaust components, over model bimetallic Pt-Pd/γ-Al<sub>2</sub>O<sub>3</sub> catalysts. During CO oxidation tests, monometallic Pt suffered the most extensive inhibition which was correlated to a greater extent of dicarbonyl species formation. Pd and Pd-rich bimetallics were inhibited by carbonate formation at higher temperatures. The 1:1 and 3:1 Pt:Pd bimetallic catalysts did not form the dicarbonyl species to the same extent as the monometallic Pt sample, and therefore did not suffer from the same level of inhibition. Similarly they also did not form carbonates to as large an extent as the Pd-rich samples and were therefore not as inhibited from this intermediate surface species at higher temperature. The Pd-rich samples were relatively poor propylene oxidation catalysts; and partial oxidation product accumulation deactivated these catalysts. Byproducts observed include acetone, ethylene, acetaldehyde, acetic acid, formaldehyde and CO. For CO and propylene co-oxidation, the onset of propylene oxidation was not observed until complete CO oxidation was achieved, and the bimetallics showed higher activity. This was again related to less extensive poisoning, less dicarbonyl species formation and less overall partial oxidation product accumulation.

© 2016 Elsevier B.V. All rights reserved.

## 1. Introduction

Increasingly stringent environmental policies due to concerns over global warming and climate change, established by agencies such as the Environmental Protection Agency (EPA), are a driving force for increasing engine fuel economy and decreasing their harmful emissions. One approach to increased fuel economies is operating under fuel lean modes, as diesel engines do, which are typically more fuel efficient than their gasoline counterparts. Furthermore, new low temperature combustion (LTC) modes being studied for diesels are even more fuel efficient.

In comparing conventional diesel combustion and two LTC technologies, reactivity controlled compression ignition (RCCI) and

premixed charge compression ignition (PCCI) [1], the LTC engine emissions have much lower NO<sub>x</sub> and particulate matter concentrations when compared to those when running the diesel engine under a normal combustion mode; however the LTC engines emitted higher concentrations of hydrocarbons and CO. This coupled with lower engine exhaust temperatures, by about 40–70 °C (since the LTC modes are more fuel efficient), puts increasing emphasis on the oxidation catalyst in the exhaust after-treatment system to oxidize CO and hydrocarbons. With regard to how these higher concentrations affect catalyst performance, for commercial Pt and Pt-Pd/Al<sub>2</sub>O<sub>3</sub> diesel oxidation catalysts (DOCs), the low CO and hydrocarbon concentrations emitted under the conventional mode reach full conversion by 190 °C, while the higher concentrations emitted with the RCCI engine resulted in full conversion near 300 °C [2].

Typical CO and hydrocarbon (HC) oxidation catalysts contain Pt and Pd; it is favorable to replace some Pt with Pd for economic rea-

\* Corresponding Author.

E-mail address: [wsepling@uh.edu](mailto:wsepling@uh.edu) (W.S. Epling).

sons, and adding Pd to Pt-based catalysts leads to less Pt sintering relative to monometallic catalysts [3–6]. It has also been shown that Pd is less sensitive to CO poisoning than Pt [7]. There is a non-linear relationship between oxidation performance and Pt or Pd content, with different Pt:Pd molar ratios achieving the lowest light-off temperatures for different compounds [8]. As an example, in a previous DOC study it was shown that a higher Pt content in bimetallic Pt/Pd catalysts led to better (lower temperature) NO, decane and propylene oxidation, while catalysts with a higher Pd content led to improved CO oxidation performance [9]. Understanding and predicting this bimetallic behavior has proven challenging as to date no apparent relationship exists between the metal properties and catalyst performance [5]. Due to the high CO and HC concentrations in LTC engine exhaust discussed above, more emphasis needs to be placed on understanding the Pt and Pd activity in the DOC.

In general, a catalyst containing a Pt and Pd blend results in improved oxidation relative to the monometallic catalysts and this has been attributed to metal alloying and bimetallic particle formation [10,11]. The bimetallic interactions are important as Pt influences the Pd oxidation state. For example, in the monometallic case Pd is completely oxidized after calcination and in the zero valent state after reduction, whereas in bimetallic catalysts both metallic and oxidized forms are present after calcination and reduction [6].

Multiple characterization techniques have been used to understand the Pt:Pd bimetallic particle structures supported on a variety of materials (SiO<sub>2</sub>, Al<sub>2</sub>O<sub>3</sub>, zeolites, carbon); such as extended X-ray absorption fine structure (EXAFS) [10,12–14], X-ray absorption near edge structure (XANES) [12], transmission electron microscopy (TEM) [10,12,13], and diffuse reflectance infrared Fourier transform spectroscopy (DRIFTS) [11]. All these techniques show that Pd segregates to the particle surfaces, leading to a Pt core surrounded by metallic Pd, or small Pd particles dispersed on the Pt core. It has also been shown that Pd surface segregation increased with particle size, and with small particle sizes Pt was also present at the surface [15]. Also, under high temperature oxidizing conditions, some metallic Pd in these bimetallic particles was oxidized into PdO clusters [16]. However, another study found that surface segregation under oxidizing conditions did not occur, and the particles appeared as alloys with PdO dispersed on the support [17]. In yet another study the authors concluded that under oxidizing conditions and with large CO concentrations in the gas phase, oxidized Pd was not the active site for CO oxidation as is often suggested, but instead the active site was metallic Pd [18].

Thus, not only does changing the Pt:Pd ratio change particle size, metal oxidation state and which metal is present at the particle surface; these properties in turn can vary as a function of reaction conditions, adding to the complexity. In this study we used chemisorption, microscopy, diffuse reflectance infrared Fourier transform spectroscopy (DRIFTS), and CO and C<sub>3</sub>H<sub>6</sub> oxidation reactor studies to better understand the catalytic activity and CO and C<sub>3</sub>H<sub>6</sub> oxidation reaction mechanisms as a function of Pt:Pd ratio.

## 2. Experimental

### 2.1. Catalyst synthesis

Monometallic Pt and Pd, and different Pt:Pd ratio bimetallic catalysts were prepared by incipient wetness impregnation on Al<sub>2</sub>O<sub>3</sub>, using Pt(NH<sub>3</sub>)<sub>4</sub>(NO<sub>3</sub>)<sub>2</sub> and Pd(NO<sub>3</sub>)<sub>2</sub> precursors. The Al<sub>2</sub>O<sub>3</sub> was supplied by SASOL Germany, the Pd(NO<sub>3</sub>)<sub>2</sub> and Pt(NH<sub>3</sub>)<sub>4</sub>(NO<sub>3</sub>)<sub>2</sub> were both purchased from Sigma Aldrich. All catalysts prepared were based on the metal molar concentration of a 1 wt% Pt catalyst loading, i.e. the monometallic Pd catalyst contained 0.55 wt%

Pd. Catalysts were dried overnight and the heated to 550 °C at a 5 °C/min ramp rate, and held at 550 °C for 4 h as the calcination step.

### 2.2. CO chemisorption

Temperature programmed desorption (TPD) after CO adsorption [19] was used to measure dispersion. These TPD experiments were done on a bench reactor setup; the total flow rate was 200 mL/min and the CO concentration in the initial adsorption stage was 7000 ppm in N<sub>2</sub> at 30 °C for 1 h, followed by only N<sub>2</sub> for 80 min to desorb the physically adsorbed CO, and then a 28 °C/min temperature ramp up to 835 °C to desorb all the chemisorbed CO. The desorbed CO was measured and used to calculate particle size. For CO a stoichiometry of 1 was assumed to calculate particle sizes. The site density for Pt and Pd were taken as 0.0800 and 0.0787 nm<sup>2</sup>/atom respectively [20].

### 2.3. Microscopy

High-angle annular dark-field and bright-field STEM images were recorded using a JEOL 2200FS FEG (S)TEM equipped with a CEOS GmbH (Heidelberg, Ger) hexapole aberration-corrector on the probe-forming lenses. Energy-dispersive x-ray spectroscopy (EDS) results were acquired from a Bruker-AXS X-Flash silicon-drift detector (SDD) mounted on the column; the 30-mm<sup>2</sup> detector provided a collection angle of <0.1 sr.

Because of the limitations of the collection efficiency for the available SDD system, spectra were recorded using a probe current of ~290 pA (i.e. using AMAG mode spot size 4C with a 26.5 mrad semi-angle probe convergence) to provide a reasonable count rate for best statistics. The Objects mode of the Bruker Esprit software was used to select a scan area to cover the entire area of e.g. a 2–5 nm catalyst particle, and a spectrum was collected for 10–30 s, a time after which the alumina support became too damaged by beam effects to reliably retain the catalyst particle. On some occasions, “hypermaps” were acquired over a larger area containing a number of catalyst particles, from which EDS quantification values could be obtained by post-processing within the Bruker ESPRIT software, using the Cliff-Lorimer method. Frequency distributions were calculated from these results. The Pt/Pd ratios for ≥10 particles in the 2–5 nm range were sorted into 5% Pt bins ranging from 27.5 to 77.5% Pt for each bimetallic catalyst. The EDS ratios were sorted into bins that were less than or equal to the bin value (i.e. ≤27.5%, >27.5% but ≤32.5%, etc.). Frequencies were calculated based on the total number of particle ratios measured for each catalyst.

### 2.4. Catalyst bench reactor testing

In reactor tests, 29.3 mg of catalyst was used. The powder material was pressed and sieved to 40–60 US sieve mesh along with SiO<sub>2</sub> particles, and placed in a 4 mm ID quartz tube reactor. The SiO<sub>2</sub> particles were purchased from Sigma Aldrich and were added, at 10× dilution by mass, to minimize temperature gradients. Quartz wool was placed on both sides of the catalyst to keep the catalyst bed stationary.

Temperature programmed oxidation (TPO) experiments were conducted with 3000 ppm CO, and/or 1500 ppm C<sub>3</sub>H<sub>6</sub> with excess O<sub>2</sub> (6 or 8 vol%) in order to approximate LTC exhaust conditions. Note that no H<sub>2</sub>O and CO<sub>2</sub> were used in these tests; while the CO<sub>2</sub> is not expected to affect the kinetics, H<sub>2</sub>O has a known effect on CO and hydrocarbon oxidation. We started with a simple kinetic study without H<sub>2</sub>O, so as to decouple any H<sub>2</sub>O effect as a function of Pt:Pd ratio on CO and hydrocarbon oxidation, and avoid water gas shift and reforming reactions complicating interpretation as well. MKS

mass flow controllers were used to control the gas flow rates to create the desired inlet gas concentrations. Inlet and outlet gas lines were heated above 100 °C, in order to avoid product water condensation on the lines. Outlet gas concentrations were measured with a MKS MultiGas 2030 FTIR gas analyzer with built in calibrations.

TPO experiments were conducted from 100 to 300 °C with a 5 °C/min ramp rate, and then the CO and/or C<sub>3</sub>H<sub>6</sub> were shut off and the ramp continued to 500 °C and held for 30 min in 10% O<sub>2</sub> and N<sub>2</sub> only, to pretreat the catalyst for the next experiment. A Thermo Scientific Lindberg Blue Minimite tube furnace was used. Prior to the temperature ramp, the reactor was held at 100 °C in order to ensure a stable inlet concentration measurement.

One thermocouple was placed ~2 cm upstream of the catalyst to measure gas inlet temperature, and one thermocouple was placed in the catalyst bed center. A 400 mL/min total flow rate was used, which corresponds to a 100,000 h<sup>-1</sup> monolith space velocity for a 2 g/in<sup>3</sup> monolith washcoat loading (292 k hr<sup>-1</sup> on a powder basis). The temperature and concentration data were averaged every 2 s, and conversion calculations were done with respect to the average inlet concentration measured over the 500 s prior to the temperature ramp. Turnover frequencies were calculated using the dispersion determined from the CO TPD experiments, and a particle molecular weight corresponding to the Pt:Pd ratio on the catalyst.

### 2.5. Diffuse reflectance infrared Fourier transform spectroscopy (DRIFTS)

In order to identify adsorbed species and possible differences in the oxidation states of the monometallic versus bimetallic samples, *in situ* DRIFTS experiments were performed using a Nicolet 6700 spectrometer equipped with a MCT detector and a high temperature Harrick Scientific Praying Mantis reaction chamber with ZnSe windows. 30 mg of catalyst was mixed with an equal amount of KBr to form the sample. The DRIFTS spectra were collected in the 4000–650 cm<sup>-1</sup> wavenumber range, accumulating 98 scans at 4 cm<sup>-1</sup> resolution.

TPO experiments were performed as part of the DRIFTS experiments. The sample was heated at 5 °C/min from 100 to 365 °C, and run such that a spectrum was obtained every 5 °C. As measured by a thermocouple placed in the gas stream, this corresponded to a 4.2 °C/min temperature ramp from 80 to 300 °C. A background spectrum was taken at the beginning of the temperature ramp in flowing He, and then the reactant gases were added and the samples were exposed to the feed gas for at least 1 h before the temperature ramp was started.

The concentrations in the DRIFTS experiments were 0 or 3000 ppm CO, 0 or 1500 ppm C<sub>3</sub>H<sub>6</sub>, with 8% O<sub>2</sub> in balance He. A 50 mL/min total flow rate was maintained using MKS mass flow controllers. TPO experiments were also performed with O<sub>2</sub> and He only so the spectral data obtained could be subtracted from the spectra obtained during the TPOs with CO, C<sub>3</sub>H<sub>6</sub>, and both CO and C<sub>3</sub>H<sub>6</sub>. This was done in order to remove any background shift due to temperature and any other temperature effects. A pretreatment before the experiments and between each TPO experiment at 500 °C with 10% O<sub>2</sub> for 30 min was used, similar to the pretreatment for the bench reactor testing.

## 3. Results

### 3.1. Catalyst characterization

The chemisorption results translated to particle sizes are listed in Table 1. These catalysts have comparable average particle sizes, all in the 1.6–3.6 nm range. The bimetallic particle compositional morphology was measured by energy-dispersive X-ray

**Table 1**

Average particle size as a function of Pt:Pd ratio as determined by CO chemisorption using 1:1 adsorption stoichiometry.

Ratio (Pt:Pd)	1:0	3:1	1:1	1:3	0:1
Particle Size [nm]	1.9	1.6	2.7	3.6	2.5

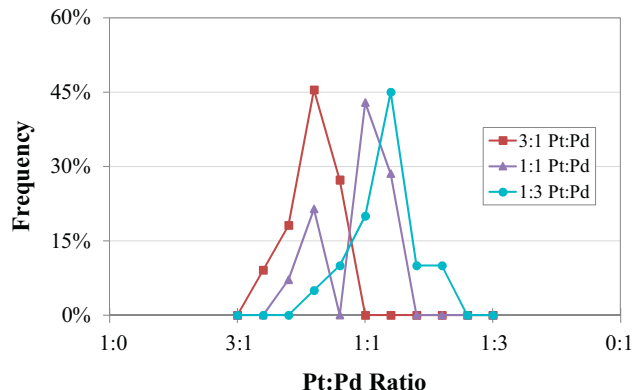


**Fig. 1.** Compositional morphology determined using energy-dispersive X-ray spectroscopy (EDS) data collected for particles in 2–5 nm range. The x-axis represents the mid-point of the frequency bin used to sort Pt/Pd atomic ratios measured by EDS.

spectroscopy (EDS), and these results are shown in Fig. 1. Low collection times were required to prevent beam-induced morphology changes to the metal particles resulting in low EDS counts, therefore the frequencies were sorted into ranges to provide more of a qualitative comparison between the different Pt:Pd catalysts. Sample loading of the TEM grids often resulted in clumping of the alumina support particles resulting in micrographs which showed both particles in the 2–5 nm range and what resemble agglomerations of particles. Many of these larger agglomerates were the result of the alumina support particles overlapping and do not represent large connected Pt:Pd particles. Therefore, to better represent the catalytically available environments only isolated particles in the 2–5 nm range were evaluated for the graph in Fig. 1. The EDS data from the 3:1 Pt-Pd catalyst particles suggests Pt-rich Pt-Pd particles; however the frequency distribution of the particles are centered slightly lower, more in the 3:2 Pt:Pd range. High resolution ACEM imaging of the 3:1 catalyst consistently shows rafts <1 nm. Platinum rafts consisting of 10–20 Pt atoms have been previously observed by ACEM on alumina supported catalysts and likely make-up the remainder of the Pt loading [21]. The 1:1 Pt-Pd catalyst appears to form predominately 1:1 Pt-Pd particles. A high frequency of the Pt-Pd particles on the 1:3 catalyst also fall in the 1:1 Pt-Pd range rather than the anticipated Pd-rich composition. This may suggest that the 1:1 Pt-Pd particles are favored over Pd-rich bimetallic particles during synthesis. The remaining Pd loading is likely present as smaller PdO particles. Longer EDS collection times over larger areas show that the overall quantification of the Pt:Pd ratios more closely match those used during synthesis, supporting the presence of Pt-only and Pd-only particles to make up the loading imbalances on the 3:1 and 1:3 catalysts. Note, these data clearly show non-uniformity in particle sizes and to some extent composition (with 2 seemingly evident for the 1:3 and 3:1 samples). Such will influence the analysis of the characterization of surface species and where they reside, and admittedly leave questions. However, the synthesis approach used is quite common/typical and thus in the simplest of context the results are meaningful from a practical viewpoint. But also, the results discussed below can be used to distinguish reactions and mechanisms, even with multiple particle types, as will be shown.

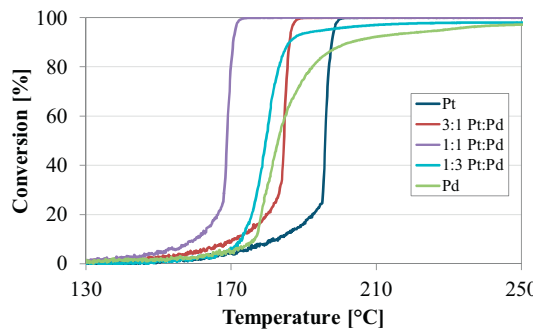


**Fig. 2.** CO conversion as a function of upstream gas temperature during TPO with ramp rate 5 °C/min for five different Pt:Pd ratios. Feed gas composition: 3000 ppm CO, 8% O<sub>2</sub> in balance N<sub>2</sub>.

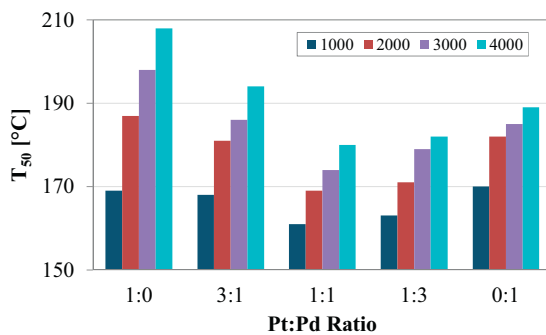


**Fig. 3.** CO oxidation performance with different CO concentrations in terms of T<sub>50</sub>, the temperature where 50% of the inlet CO is oxidized. Feed gas composition: 1000–4000 ppm CO, 6% O<sub>2</sub>, balance N<sub>2</sub>.

### 3.2. CO oxidation results

#### 3.2.1. Reactor testing

The CO oxidation conversion data are shown in Fig. 2. The conversion versus temperature profiles for the Pt, 3:1 and 1:1 Pt:Pd catalysts have a much steeper slope above 20% conversion than the Pd and 1:3 Pt:Pd catalysts. Also, the light-off temperatures for the bimetallic catalysts are generally lower than those for the monometallic catalysts. In evaluating the turnover frequencies, shown in Fig. S1, no differences in trends are observed. Full CO conversion over the 1:3 Pt:Pd and the monometallic Pd catalyst was not attained, even at high temperature.

The temperatures corresponding to 50% CO conversion, T<sub>50</sub>, where 4 different CO inlet concentrations were used in the inlet gas are shown in Fig. 3. The difference in CO oxidation performance between the monometallic Pt and Pd samples increased as the CO concentration increased; the monometallic Pt catalyst performance was nearly identical to that of the Pd for 1000 ppm CO, but the successive increases to 2000, 3000 and 4000 ppm CO led to 5 °C, 13 °C, and 19 °C differences between the Pt and Pd catalyst T<sub>50</sub> values. For the bimetallic samples, there were also some differences in T<sub>50</sub> with CO concentration increase. If a performance ranking in terms of T<sub>50</sub> is used, it changes as a function of CO concentration. For all concentrations, the 1:1 and 1:3 Pt:Pd catalysts result in the best and second best performance in terms of T<sub>50</sub>, respectively. The 3:1 and monometallic Pt catalyst T<sub>50</sub> values are lower than that of the Pd catalyst at low CO concentrations, but then their performance falls below the monometallic Pd catalyst at 2000 ppm for the Pt catalyst and 3000 ppm for the 3:1 Pt:Pd catalyst.

#### 3.2.2. DRIFTS experiments

DRIFTS was used to characterize CO interactions with the catalyst surfaces during adsorption and TPO experiments, using a

similar approach to that taken with a monometallic Pt catalyst [22]. The DRIFTS spectra obtained after sample exposure to CO and O<sub>2</sub> at 80 °C for 1 h are shown in Fig. 4 a), and the species represented by the spectral features are labeled based on literature results. The small feature at ~2200 cm<sup>-1</sup> corresponds to CO on Lewis acid sites [23], and is not considered catalytically important. In comparing the Pt catalyst to the Pd catalyst, there were large differences in the amounts of linear bound carbonyl and triply bound CO between the two. The Pd contained less linearly bound and more triply bound, with also some bridge bound carbonyls (at 1930 cm<sup>-1</sup>). This is consistent with the Pd(111) crystal structure, where Pd(100) would favor linearly bound carbonyls, and Pd(111) favors triply bound CO in the three fold hollow sites [7,18,24]. Both of these linearly bound CO features commonly appear with high CO concentrations and the resulting high CO coverages. The lower wavenumber linear carbonyl peak, around 2090 cm<sup>-1</sup>, is assigned as a single linear carbonyl (labeled as CO-M in subsequent figures, where M represents Pd or Pt), and the higher wavenumber feature at 2111 cm<sup>-1</sup> (labeled as CO-M-O in subsequent figures) indicates either a dicarbonyl [25–28], which has been observed on small particles or atomic Pt, or a linear carbonyl attached to a Pt that is also attached to atomic oxygen [21,29–31]. If the 2111 cm<sup>-1</sup> peak corresponded to a dicarbonyl, another dicarbonyl feature should be observed at 2050 cm<sup>-1</sup>. Calculated relative CO-associated peak heights indicate that the 2050 cm<sup>-1</sup> peak (hereafter labeled as CO-M-CO) is not large enough in comparison to the 2111 cm<sup>-1</sup> peak for this peak to correspond to only the dicarbonyl species. For instance, in comparing the Pt catalyst to the 1:1 Pt:Pd catalyst, the relative height of the CO-M-O was 230% larger, while the relative height of the

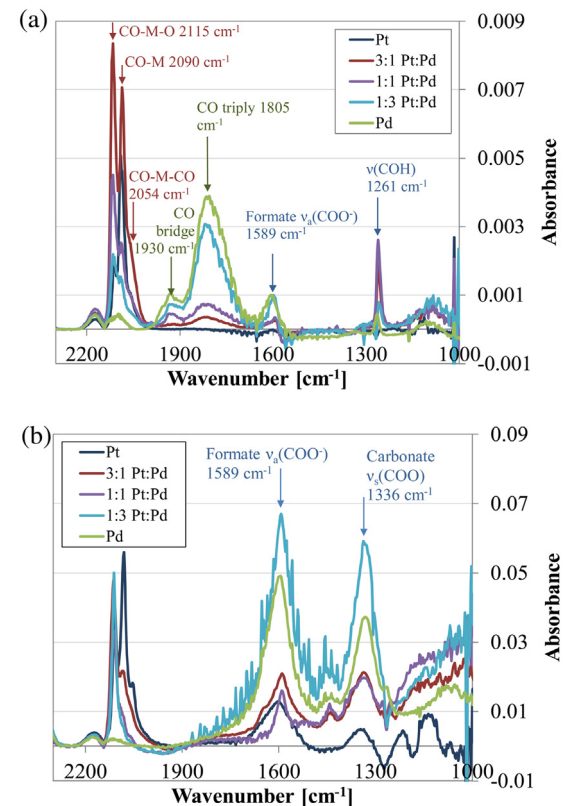


**Fig. 4.** DRIFTS spectra obtained during catalyst exposure to CO and O<sub>2</sub> at a) 80 °C and b) 200 °C, with 98 scans at 4 cm<sup>-1</sup> resolution in the 2300–1000 cm<sup>-1</sup> region. Reference wavenumbers: CO-M-CO 2054 cm<sup>-1</sup>, CO-M 2090 cm<sup>-1</sup>, CO-M 2115 cm<sup>-1</sup>, CO bridge 1930 cm<sup>-1</sup>, CO triply 1805 cm<sup>-1</sup>, formate ν<sub>4</sub>(COO<sup>-</sup>) 1589 cm<sup>-1</sup>, monodentate carbonate 1336 cm<sup>-1</sup> ν<sub>5</sub>(COO<sup>-</sup>). Feed gas composition: 3000 ppm CO, 8% O<sub>2</sub>, balance He; 1 h exposure time before 4.2 °C/min temperature ramp.

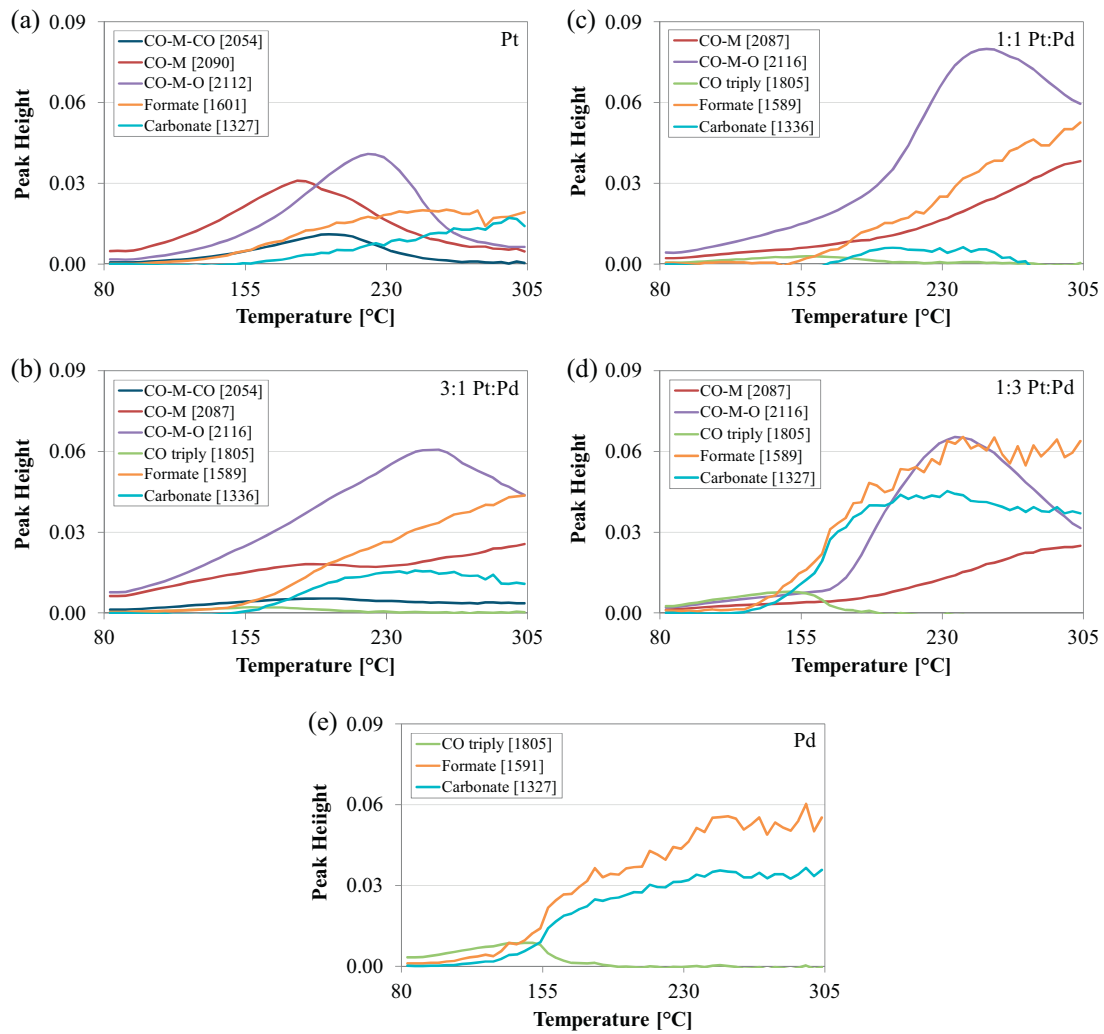


**Fig. 5.** Peak height as a function of gas stream temperature for peaks of interest in CO oxidation [wavenumber in  $\text{cm}^{-1}$ ]. Feed gas composition: 3000 ppm CO, 8%  $\text{O}_2$ , balance He. (a) Pt, (b) 3:1 Pt:Pd, (c) 1:1 Pt:Pd, (d) 1:3 Pt:Pd, (e) Pd.

CO–M–CO peak was 25% smaller, which clearly indicates that the  $2111\text{ cm}^{-1}$  corresponds to something other than only dicarbonyl. Therefore the  $2111\text{ cm}^{-1}$  peak has been interpreted as CO–M–O where the carbonyl is adsorbed with atomic oxygen on a metal site, either Pt or Pd. Both the 3:1 Pt:Pd and monometallic Pt catalysts had large linear carbonyl features, but they differed in type. The monometallic sample formed the most CO–M, whereas the 3:1 formed the most CO–M–O. The 1:1 catalyst formed a large amount of both linear carbonyl in CO–M–O configuration and bridged carbonyl species.

The carbonate and carboxylate peak assignments in the  $1800\text{--}1000\text{ cm}^{-1}$  range are as follows. The anticipated species for CO oxidation include formate, free carbonate ions, monodentate carbonate, bidentate carbonate, bicarbonate, and COH species. For the formate species, the peaks identified from literature are  $\nu(\text{C--H})$  at  $2962\text{ cm}^{-1}$ ,  $\nu_a(\text{COO}^-)$  at  $1600\text{ cm}^{-1}$ , and  $\nu_s(\text{COO}^-)$  at  $1394$  or  $1363\text{ cm}^{-1}$  [23,32–34]. For the free carbonate ion, the peaks are  $\nu_a(\text{CO}_3^{2-})$  at  $1450\text{--}1420$  and  $\nu_s(\text{CO}_3^{2-})$  at  $1090\text{--}1020\text{ cm}^{-1}$  [34,35]. For the monodentate carbonate, the peaks are  $\nu_a(\text{COO})$  at  $1530\text{--}1470$ ,  $\nu_s(\text{COO})$  at  $1300\text{--}1370$ , and  $\nu(\text{C--O})$  at  $1080\text{--}1040\text{ cm}^{-1}$  [34,36]. For the bidentate carbonate, the peaks are  $\nu(\text{C=O})$  at  $1530\text{--}1620$  or  $1620\text{--}1670$ ,  $\nu_a(\text{COO})$  at  $1270\text{--}1250$  or  $1220\text{--}1270$ , and  $\nu_s(\text{COO})$  at  $1030\text{--}1020$  or  $980\text{--}1020\text{ cm}^{-1}$  [34,36]. For bicarbonate, the peaks are  $\nu(\text{C=O})$  at  $1640\text{--}1650$ ,  $\nu_a(\text{COO})$  at  $1430\text{--}1470$ ,  $\nu_s(\text{COO})$  at  $1304$ , and  $\nu(\text{COH})$  at  $1230\text{ cm}^{-1}$  [23,37–39]. For COH, the peak for  $\nu(\text{COH})$

is at  $1270\text{ cm}^{-1}$ ; and for HCOH, a bending mode occurs at  $1200\text{ cm}^{-1}$  [40]. Many of these peaks for the species mentioned overlap, however using some process of elimination and considering the results in Fig. 4 a) allows distinctions to be made. The observed peaks at  $1601\text{--}1589\text{ cm}^{-1}$ , together with that at  $2962\text{ cm}^{-1}$  and a broad peak around  $1370\text{--}1320\text{ cm}^{-1}$  indicate that there may be formate present. For monodentate carbonate, while there were peaks in the  $1300\text{--}1370$  and  $1080\text{--}1040$  regions, there was not a peak at  $1530\text{--}1470\text{ cm}^{-1}$  and so this species can be eliminated. For bidentate carbonate, the  $\nu(\text{C=O})$  of the bidentate was close to the  $\nu_a(\text{COO}^-)$  of formate, and if present we would expect to see peaks at  $1270\text{--}1220$  and  $1080\text{--}1040\text{ cm}^{-1}$ , both of which were observed at  $80\text{ }^\circ\text{C}$  and so this surface species is also possible. For the bicarbonate, the peaks anticipated are similar to bidentate carbonate, with the exception of  $\nu_a(\text{COO})$  at  $1430\text{--}1470$ , and  $\nu_s(\text{COO})$  at  $1304$ . There were no peaks in the  $1430\text{--}1470$  region, and so this bicarbonate species can be eliminated. This leaves formate and bidentate carbonate as possible species that were observed at the beginning of the temperature ramp. These species changed in amount, and other surface species formed, during the temperature ramp, with the spectra obtained at  $200\text{ }^\circ\text{C}$  shown in Fig. 4b). A small peak at  $1456\text{ cm}^{-1}$  appeared, and the peaks already discussed increased in intensity. The peak at  $1456\text{ cm}^{-1}$  may indicate either free carbonate ions, monodentate carbonates, or bicarbonate. Due to the absence of peaks in the  $1220\text{--}1270\text{ cm}^{-1}$  range it

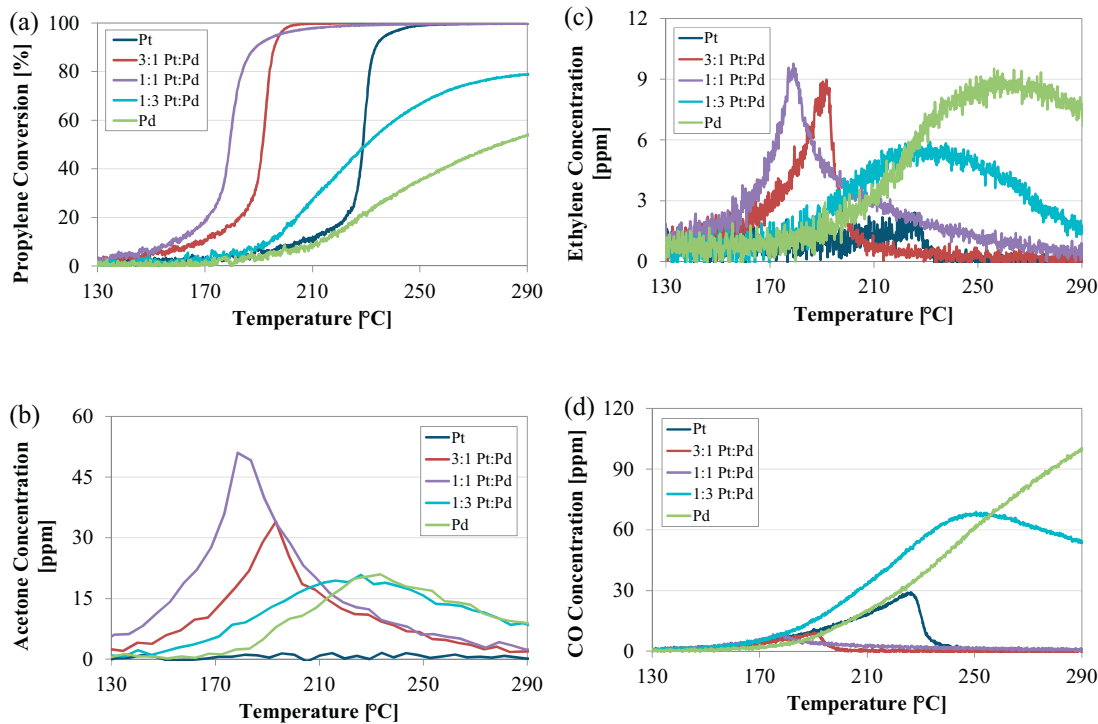


**Fig. 6.**  $\text{C}_3\text{H}_6$  oxidation performance as a function of upstream gas temperature during TPO with a ramp rate  $5\text{ }^\circ\text{C}/\text{min}$ . Feed gas composition:  $1500\text{ ppm C}_3\text{H}_6$ ,  $8\% \text{ O}_2$  in balance  $\text{N}_2$ . (a) Propylene conversion, (b) acetone concentration, (c) ethylene concentration, (d) CO concentration.

should not be bicarbonate species; this peak disappeared quickly during the temperature ramp and so this also allows us to identify the  $1600\text{ cm}^{-1}$  feature that was at first assigned to either formate or bidentate carbonate to formate only. With the peak at  $1456\text{ cm}^{-1}$ , the peak at  $1327\text{--}1336\text{ cm}^{-1}$  is assigned to the monodentate carbonate species; the expected peaks for formate in this region would be at a slightly higher wavenumber, and in addition we will see that the trends with temperature of these two peaks vary and so we can differentiate them as being related to the different species. Thus the only two peaks in the carbonate/carboxylate region discussed further are the peak at  $1589\text{--}1601\text{ cm}^{-1}$  associated with formate's  $\nu_a(\text{COO}^-)$  and the peak at  $1327\text{--}1336\text{ cm}^{-1}$  associated with monodentate carbonate's  $\nu_s(\text{COO})$ .

The key feature heights identified above were measured and used to track relative amounts on the surface as a function of temperature, with these results shown in Fig. 5. In comparing the results of the monometallic samples in Fig. 5 a) and e), formate and carbonate species were formed in greater quantity on the Pd sample relative to the Pt sample. For the bimetallic catalysts in Fig. 5 b)–d), with increasing Pd content, the formate and carbonate peak heights increased. For the Pt, 3:1 Pt:Pd, and 1:1 Pt:Pd catalysts there is a much stronger formate feature relative to carbonate. The height of the various carbonyl species on the catalysts all have maxima at different temperatures; the maxima of the linearly adsorbed species are at higher temperatures than the triply adsorbed species. As the Pd content increased, less CO–M–CO was detected and more triply bound CO was present. The CO–M–O was the largest peak for the 1:1 Pt:Pd catalyst at elevated temperatures, while the same sample had the smallest carbonate peak height through the temperature ramp.

### 3.3. $\text{C}_3\text{H}_6$ oxidation results

#### 3.3.1. Reactor testing

Propylene oxidation performance as a function of temperature and the different Pt:Pd ratios is shown in Fig. 6 a) for one  $\text{C}_3\text{H}_6$

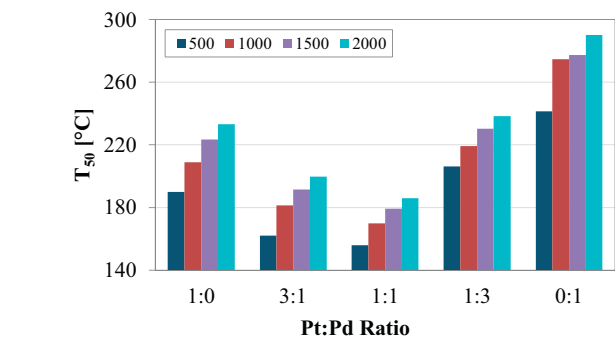


**Fig. 7.**  $\text{C}_3\text{H}_6$  oxidation performance at different  $\text{C}_3\text{H}_6$  concentrations in terms of  $T_{50}$ . Feed gas composition:  $500\text{--}2000\text{ ppm C}_3\text{H}_6$ ,  $8\% \text{ O}_2$ , balance  $\text{N}_2$ .

concentration level. The oxidation performance follows a similar trend as observed for CO oxidation in that the bimetallic catalysts showed better performance relative to the monometallic samples. Here though, the Pt catalyst was better than Pd, which was expected as Pt is generally a better alkene hydrocarbon oxidation catalyst than Pd [8]. Oxidation light off occurred at a lower temperature with the 1:1 Pt:Pd than the 3:1 Pt:Pd catalyst, however the 3:1 Pt:Pd catalyst reached full conversion at a lower temperature. The 1:3 Pt:Pd catalyst performance was similar to the Pd catalyst with just a slightly lower light off temperature and it reached a point where the conversion plateaued and did not improve any further as the temperature was increased. In comparing the  $T_{50}$  values for different propylene concentrations, Fig. 7, a clear trend exists where an increase in concentration impacts the  $T_{50}$  monotonically for each sample. Over this concentration range, the catalyst performance ranking did not change as it did for CO oxidation, and in all cases the 1:1 Pt:Pd ratio catalyst performed the best. The performance ranking for propylene oxidation for all concentrations is  $1:1 > 3:1 > 1:0 > 1:3 > 0:1 \text{ Pt:Pd}$ .

Propylene partial oxidation products vary depending on the catalyst used; for Pt and Pd supported on silica catalysts, partial oxidation products include acetaldehyde, acetic acid, acrolein, acetone and various  $C_3$  acids [41]. However the support is important; as one example acrolein was an abundant product from Au supported on  $SiO_2$  catalyst, while with Au on an  $\alpha-Al_2O_3$  support much lower acrolein concentrations were observed [42]. In this study, although acrolein was not observed, there was evidence of ethylene, acetaldehyde, formaldehyde, acetic acid, and acetone. In evaluating partial oxidation product formation as a function of Pt:Pd ratio the most abundant products were acetone, ethylene and CO, presented in Figs. 6 b), c) and d) respectively. The acetaldehyde and acetic acid formation data are provided in Supplemental Information Figs. S2 a) and b), respectively. Acetaldehyde formation over each catalyst was around 5–10 ppm with no discernable trend with Pt:Pd ratio. Acetic acid formation was less than 4 ppm, and the 1:3 Pt:Pd catalyst produced the most while the monometallic Pt sample did not catalyze formation of any. CO and ethylene formation increased as the Pd content increased; the 1:3 and monometallic Pd samples catalyzed some formaldehyde formation as an additional partial oxidation product at higher temperatures but at very low concentrations, 1–2 ppm.

### 3.3.2. DRIFTS experiments

In order to identify which partial oxidation products formed on the catalyst surface we needed to distinguish the reactant propylene from possible partial oxidation products, i.e. acrolein, acetone, acetic acid, ethylene and acetaldehyde. The complete set of peak assignments for the various surface species anticipated are compiled in Supplemental Information Table S1. Focusing first on propylene, there are three configurations by which propylene can adsorb to the surface;  $\pi$ -propylene, di- $\sigma$ -propylene, and propylidyne [43]. The various CH stretching peaks in the 2800–3100  $cm^{-1}$  range can be used to distinguish which configuration adsorbed. The spectra obtained at 80  $^{\circ}C$  are shown in Fig. 8 a). There were peaks at 2962 and 2906  $cm^{-1}$ ; from Table S1 these correspond to the  $\nu_a(CH_3)$  and  $\nu_s(CH_3)$  of propylidyne, respectively. Another peak at 1124  $cm^{-1}$  was present, but not shown in the spectra, which corresponds to  $\nu(C-C)$  of propylidyne. The peaks expected above 3000  $cm^{-1}$  for  $\pi$ -propylene were not present; which is consistent with the absence of acrolein byproduct, since mechanistically it is formed through  $\pi$ -allylic complexes [44].

The peak assignments for acetone, acrolein, acetate, and the various configurations of ethylene are listed in Table S1. Peaks in the 1200–1800  $cm^{-1}$  range were used to distinguish which oxidation products evolved at higher temperatures, and spectra obtained at 229  $^{\circ}C$  as examples are shown in Fig. 8 b). For clarity only the spectra for the monometallic Pt and Pd catalysts and 1:1 Pt:Pd are shown. Peaks at 1649, 1574, 1450, 1394, 1335, 1267  $cm^{-1}$  were observed. The peaks at 1574 and 1450  $cm^{-1}$  were evident with the 1:1 Pt:Pd and Pd samples, at similar ratios and correspond to the  $\nu_a(COO^-)$ , and  $\nu_s(COO^-)$  modes of the acetate species, respectively [45,46]. The remaining peaks at 1649, 1394, and 1335 could be the  $\nu(C=O)$ ,  $\delta_a(CH_3)$  and  $\delta_s(CH_3)$  acetone bands, respectfully [47]. While there are several similar IR features between acrolein and acetone, the characteristic  $\nu(C=O)$  at 1700  $cm^{-1}$  for acrolein was not observed [48]. Since we observed ethylene as a partial oxidation product, the peaks for the three configurations of ethylene are also listed in Table S1;  $\pi$ -ethylene, di- $\sigma$ -ethylene, and ethylidyne [49]. None of the peaks in the DRIFTS results are attributed to the first two configurations of ethylene, however the peaks associated with propylidyne are common to ethylidyne and so the increase in intensity of these peaks with temperature could be associated with ethylidyne as well. The presence of the  $\nu(COH)$  is at 1267  $cm^{-1}$  on the 1:1 and Pd sample at 229  $^{\circ}C$ , with the acetate peaks, may also indicate the

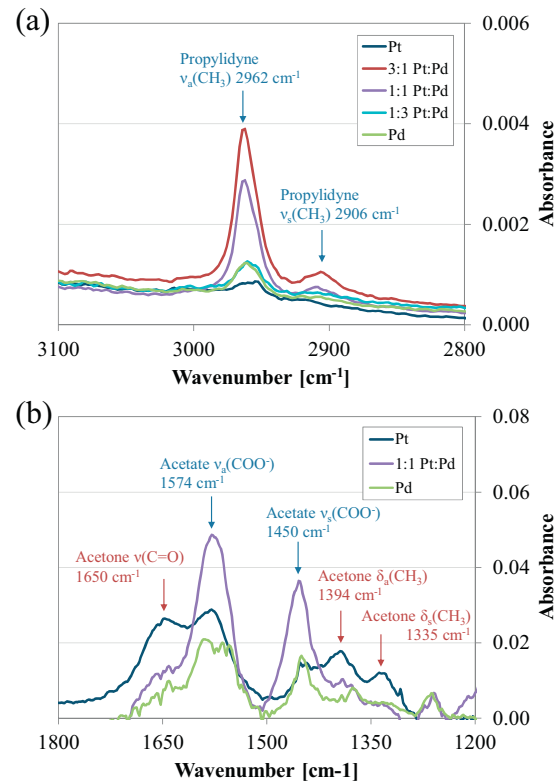


**Fig. 8.** DRIFTS spectra obtained during catalyst exposure to  $C_3H_6$  and  $O_2$  at a) 80  $^{\circ}C$  and b) 229  $^{\circ}C$ , with 98 scans at 4  $cm^{-1}$  resolution in the 2300–1000  $cm^{-1}$  region. Reference wavenumbers: acetone 1649  $cm^{-1}$ , acetate 1450  $cm^{-1}$ , propylidyne 2962 and 2906  $cm^{-1}$ . Feed gas composition: 1500 ppm  $C_3H_6$ , 8%  $O_2$ , balance He; 1 h exposure time before 4.2  $^{\circ}C/min$  temperature ramp.

formation of acetic acid, which is consistent with observations from the reactor testing.

Summarized DRIFTS data obtained from the propylene oxidation experiments are shown in Fig. 9, where the acetone  $\nu(C=O)$  1649  $cm^{-1}$  peak, the acetate  $\nu_s(COO^-)$  1450  $cm^{-1}$  peak, and the linear carbonyl 2111  $cm^{-1}$  peak are plotted as a function of inlet gas temperature. The  $\nu_s(COO^-)$  peak at 1450  $cm^{-1}$  for acetate was chosen, since the 1574  $cm^{-1}$  feature is near that of a formate peak (1587–1600  $cm^{-1}$ ) that was observed during CO oxidation, and thus difficult to assign during co-oxidation experiments discussed below. The propylidyne or ethylidyne 1124  $cm^{-1}$   $\nu(C-C)$  mode as a function of temperature is plotted in Fig. S3, and increased with temperature for the Pt catalyst but did not increase significantly on the other catalysts. The acetic acid  $\nu(COH)$  mode at 1267  $cm^{-1}$  is not plotted as a function of temperature; this peak was observed and increased with temperature for the 3:1 and 1:1 Pt:Pd catalysts, however there was a maxima which did not follow the acetate peak. This may indicate that on the 1:1 and 3:1 Pt:Pd catalysts there was an intermediate temperature range where acetic acid was formed, which is consistent with the reactor testing. The CO–M–CO peak at 2050  $cm^{-1}$  was not observed, and so the 2111  $cm^{-1}$  peak has been attributed to CO–M–O species. Relating these data to the reactor testing, the oxidation onset can be identified by CO formation on the surface, based on the observation from the reactor tests where CO was observed once propylene oxidation commenced. With this indicator, surface CO formation occurred just prior to the temperature where the acetone and acetate related peaks started to increase in intensity. This confirms the association of these peaks with partial oxidation intermediates and not from propylene adsorption on the active sites via  $\pi$  or  $\sigma$  bonding.

**Table 2**

$T_{50}$  (temperature at 50% conversion) for CO and  $C_3H_6$  as individual reactants and during co-oxidation; feed gas concentrations as labeled with 8%  $O_2$  in balance  $N_2$ .

Ratio (Pt:Pd)	3000 ppm CO $T_{50}$ [°C]	1500 ppm $C_3H_6$ $T_{50}$ [°C]	3000 ppm CO and 1500 ppm $C_3H_6$	
	$T_{50}$ CO [°C]	$T_{50}$ $C_3H_6$ [°C]		
1:0	196	223	296	304
3:1	184	191	218	219
1:1	169	179	196	196
1:3	180	230	208	245
0:1	183	277	–	–

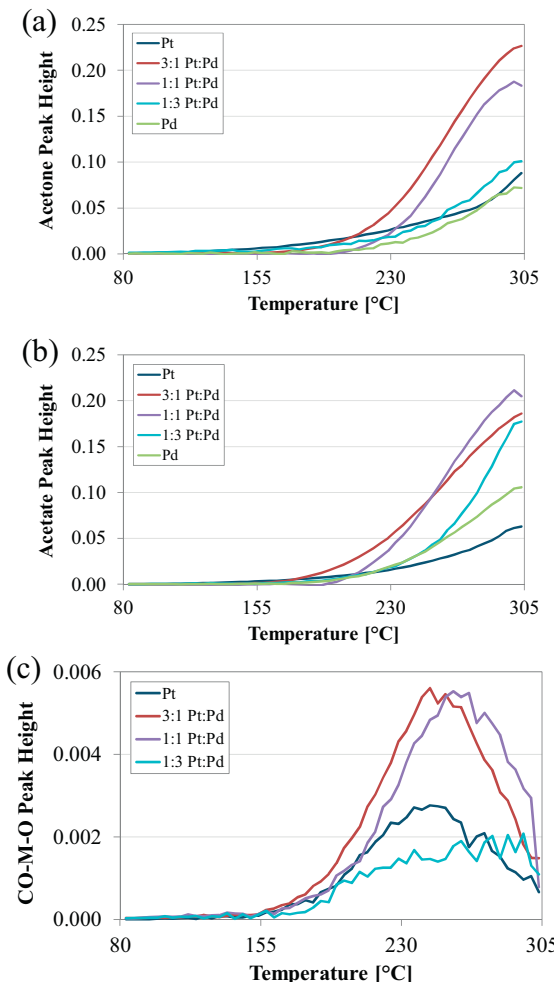


**Fig. 9.** Peak height as a function of gas stream temperature for peaks of interest in  $C_3H_6$  oxidation. Feed gas composition: 1500 ppm  $C_3H_6$ , 8%  $O_2$ , balance He. (a) acetone [1649 cm<sup>-1</sup>], (b) acetate [1450 cm<sup>-1</sup>], (c) linear carbonyl CO–M–O [2111 cm<sup>-1</sup>].

The partial oxidation products from the reactor testing and DRIFTS tests correlate quite well. From the reactor testing, Fig. 6 b), all the samples led to acetone formation, with the most formed over the 1:1 Pt:Pd catalyst. Surface acetone formation, in Fig. 9 a), followed a similar trend; acetone formation was observed to the largest extent on the 3:1 and 1:1 catalysts. Acetone formation was observed on the surface of the Pt catalyst, but was not present in the gas phase products. From the reactor testing, the Pd-containing catalysts formed the most ethylene, as shown in Fig. 6 c). Ethylene formation could be related to the ethylidyne species, which did not increase as a function of temperature for the Pd catalyst, or the acetate species observed on the surface, shown in Fig. 9 b), where more formed on the catalysts with a high Pd content, which agrees with reactor results. The CO concentrations from the reactor testing are shown in Fig. 6 d), and were the lowest from the 1:1

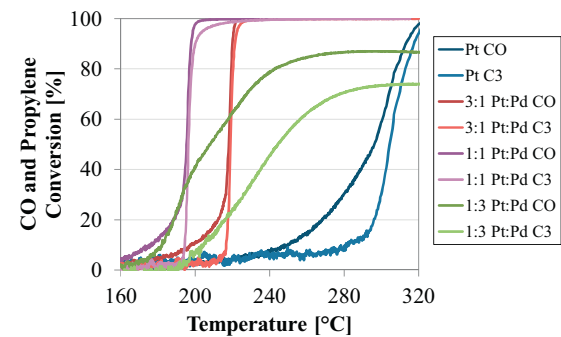


**Fig. 10.** CO and  $C_3H_6$  conversion as a function of upstream gas temperature during TPO with a ramp rate 5 °C/min. Feed gas composition: 3000 ppm CO, 1500 ppm  $C_3H_6$ , 8%  $O_2$  in balance  $N_2$ .

Pd:Pd and 3:1 Pt:Pd catalysts. The trends observed in the DRIFTS, Fig. 9 c), demonstrate that the CO–M–O peak heights during  $C_3H_6$  oxidation go through a maximum for Pt, 3:1 Pt:Pd and 1:1 Pt:Pd catalysts, which was also observed in reactor testing. The highest amount of CO formed on the 3:1 and 1:1 Pt:Pd catalyst surfaces, which also catalyzed the lowest effluent CO concentrations during reactor testing.

### 3.4. CO and $C_3H_6$ Co-oxidation results

#### 3.4.1. Reactor testing

CO and propylene co-oxidation performance was also evaluated and representative data are shown in Fig. 10. The monometallic Pd catalyst performance is not presented, as stable performance between TPO experiments was not attained under these conditions; loss in performance was continuously noted when running repeat experiments to verify reproducibility. All other catalyst resulted in repeatable data, as did the monometallic Pd sample in CO or  $C_3H_6$  oxidation testing. From the conversion data shown in Fig. 10, the 1:1 Pt:Pd catalyst was again the best sample, with low temperature light off and rapid acceleration to high conversion for both CO and propylene. The ignition slope for the 3:1 Pt:Pd catalyst was steeper, and the 1:3 Pt:Pd sample resulted in a lower CO light off temperature required compared to the 3:1 sample, but the ignition slope was much shallower and propylene oxidation occurred at a much higher temperature.

For comparison purposes, the  $T_{50}$  values for CO and  $C_3H_6$  during co-oxidation and individual component oxidation for the catalysts are tabulated in Table 2. The 1:3 sample had the largest difference between the CO  $T_{50}$  and the propylene  $T_{50}$  during co-oxidation. The catalyst performance ranking for co-oxidation in terms of CO  $T_{50}$  is 1:1 Pt:Pd > 1:3 Pt:Pd > 3:1 Pt:Pd > 1:0 Pt:Pd, and in terms of propylene  $T_{50}$  is 1:1 Pt:Pd > 3:1 Pt:Pd > 1:3 Pt:Pd > 1:0 Pt:Pd.

Propylene partial oxidation product formation results are shown in Supplemental Information Fig. S4. With CO present there were in general less partial oxidation products formed. Ethylene formation reached a 4 ppm maximum for the 1:1 and 1:3 Pt:Pd catalysts and acetone formation reached a maximum of 12, 10 and 6 ppm for the 1:1, 1:3, and 3:1 Pt:Pd catalysts, respectively. Acetone

and ethylene formation peaked shortly after propylene oxidation onset, while the formation of acetaldehyde, and acetic acid for the 1:3 Pt:Pd catalyst, remained relatively constant with temperature once propylene oxidation began. Much like propylene oxidation in the absence of CO, the lowest concentrations of partial oxidation products were observed from the Pt catalyst. In the presence of CO, only the 1:3 Pt:Pd catalyst yielded acetic acid.

#### 3.4.2. DRIFTS experiments

The DRIFTS results for CO and  $C_3H_6$  co-oxidation are summarized in Fig. 11. The peaks for the CO species occurred at lower wavenumbers, as is expected [29] with propylene in the feed, and therefore peak heights were based on these lower wavenumbers. All the surface species that were observed during the individual CO or propylene oxidation experiments were here again observed. The peaks plotted in Fig. 11 are the acetone  $\nu(C=O)$   $1653\text{ cm}^{-1}$ , acetate  $\nu_s(COO^-)$   $1450\text{ cm}^{-1}$ , formate  $\nu_a(COO^-)$   $1600\text{ cm}^{-1}$ , CO-M-CO  $2054\text{ cm}^{-1}$ , CO-M  $2084\text{ cm}^{-1}$ , CO-M-O  $2112\text{ cm}^{-1}$ , and triply adsorbed CO  $1805\text{ cm}^{-1}$  peaks. Note the peak at  $1600\text{ cm}^{-1}$  is very close to the  $1574\text{ cm}^{-1}$  acetate  $\nu_a(COO^-)$  peak; once the peak at  $1450\text{ cm}^{-1}$  developed, the peak at  $1600\text{ cm}^{-1}$  slowly shifted to the lower wavenumber of acetate and the peak associated with the formate  $\nu_s(COO^-)$  at  $1342\text{ cm}^{-1}$  disappeared. Also, the peaks at  $1390$  and  $1330$  associated with the  $\delta_a(CH_3)$  and  $\delta_s(CH_3)$  of acetone appeared together with the appearance of  $\nu(C=O)$  at  $1653\text{ cm}^{-1}$ . For this case, the peak at  $1329\text{ cm}^{-1}$  associated with monodentate carbonate formation during CO oxidation did not show a trend with Pt:Pd ratio, and also interfered with the acetone  $\delta_s(CH_3)$  mode at  $1330\text{ cm}^{-1}$ , and so is not plotted in Fig. 11. The peak at  $1267\text{ cm}^{-1}$  was not observed during co-oxidation, and similar to propylene oxidation in the absence of CO, the  $1124\text{ cm}^{-1}$   $\nu(C-C)$  mode of propylidene or ethylidene as a function of temperature increased with the Pt catalyst but did not increase significantly for the other catalysts. The characteristic  $\nu(C=O)$  at  $1700\text{ cm}^{-1}$  for acrolein or other aldehydes was not observed [48,50].

## 4. Discussion

### 4.1. Catalyst characterization

The EDS data, presented in Fig. 1, suggested that monometallic Pd particles exist on the 1:3 Pt:Pd sample, which is supported by the DRIFTS data where triply bound CO features were observed, Fig. 4. Based on the DRIFTS results, where the bimetallic catalysts with a higher Pd content had more doubly and triply bound carbonyls, the 1:1 stoichiometry assumed for the CO chemisorption experiments may not be accurate. It is difficult to relate DRIFTS results to surface concentrations, however a rough estimate for bimetallic Pt:Pd catalysts and the differently adsorbed carbonyls has been evaluated in other studies. The extinction coefficient of the linear carbonyl can be 2 to 3 times higher than that of the bridged species [51]. In other studies, this information has been used to calculate surface compositions of Pt-Pd catalysts [12,51]; however in these studies triply bound species were not observed. Here, we used this information to calculate the relative amounts the observed species, but had to assume that the triply bound species have a similar extinction coefficient to that of the bridged species. If we continue with assumptions, that the oxygen and temperature difference during CO adsorption will not drastically alter the ratios of these species, new values for the CO stoichiometry can be calculated and used to recalculate particle sizes. Using the data obtained at  $80^\circ\text{C}$ , and that the extinction coefficient for linearly adsorbed CO is 2.5 times greater than bridged or triply bound CO, the relative amounts of each species, the stoichiometry, and a corrected particle size for each catalyst has been calculated and the results

**Table 3**

Fractions of linearly, doubly, and triply bound CO on Pt:Pd catalysts, estimated CO stoichiometry Pt:CO, and revised estimates of average particle sizes.

Ratio (Pt:Pd)	1:0	3:1	1:1	1:3	0:1
CO-M-CO [%]	6	7	4	2	0
CO-M [%]	57	38	21	10	4
CO-M-O [%]	14	40	38	15	3
Doubly [%]	23	12	24	22	26
Triply [%]	0	4	12	51	67
Stoichiometry	1.20	1.15	1.47	2.24	2.60
Particle size [nm]	1.6	1.4	1.8	1.6	1.0

are listed in Table 3. This estimated correction actually decreases the particle size range, mainly influenced by the stoichiometry correction for Pd rich catalysts since they have the multiply adsorbed CO molecules.

### 4.2. CO oxidation

In terms of CO oxidation, the bimetallic catalysts were superior to the monometallic catalysts. The 1:1 Pt:Pd catalyst resulted in the lowest  $T_{50}$  for all concentrations tested and had a steep ignition slope reaching full conversion at the lowest temperatures. While the 1:3 Pt:Pd catalyst reached  $T_{50}$  at lower temperatures than the 3:1 Pt:Pd catalyst, it did not reach full conversion. Similarly comparing the Pd and Pt catalyst, the Pd catalyst reached  $T_{50}$  at lower temperatures than the Pt catalyst but did not reach full conversion. The decrease in performance ranking for the Pt catalyst observed as the CO concentration increased is consistent with Pt being more sensitive to CO poisoning [7]. By extension this also extrapolated to the Pt-rich samples, which explains why as the CO concentration increased, performance ranking in terms of  $T_{50}$  changed.

The differently adsorbed CO species observed via DRIFTS provide some insight into the reason for the performance order change. The 1:1 and 3:1 Pt:Pd catalyst surfaces had a relatively larger amount of CO-M-O species, while the Pt catalyst did for the CO-M species and the Pd and 1:3 Pt:Pd had more triply bound and bridge bound CO. If the triply and bridge bound species were solely responsible for low temperature CO oxidation, the Pd catalyst would be expected to have the lowest temperature oxidation activity. Instead it appears that the CO-M-O species are linked to the low temperature CO oxidation activity. The CO-M-CO species is included in plots where it was significant, which was the case for the monometallic Pt catalyst where the CO-M-CO peak was present during CO light off and reached a maximum before the CO-M-O did. These results also coincide with the reactor data where the Pt catalyzed light off later than the other catalysts, demonstrating more significant CO poisoning. The single carbonyls (CO-M and CO-M-O) formed on the 1:1 catalyst grew in concentration with increasing temperature, and when the CO-M-O peak started to decrease the CO-M continued to increase. In contrast, for the Pt sample the CO-M species peaked at a lower temperature relative to the CO-M-O. The single linearly bound CO trends are manifested in the 3:1 Pt:Pd catalyst as a combination of the two samples, where a maximum was observed, then an increase at the higher temperatures. This implies that both individual Pt particles must exist in addition to the bimetallic particles, further agreeing with the results from the EDS data, which suggested that the bimetallic particles, while Pt-rich, did not account for all of the Pt loaded on the catalyst. The 1:1 Pt:Pd catalyst had the best low temperature performance, exceeding that of the 3:1 catalyst even though from the DRIFTS data the 3:1 Pt:Pd catalyst had the highest CO-M-O peak height at low temperatures. This may be due to the higher amount of CO-M observed on the 3:1 Pt:Pd catalyst as well, implying the surface is relatively more heavily covered by CO.

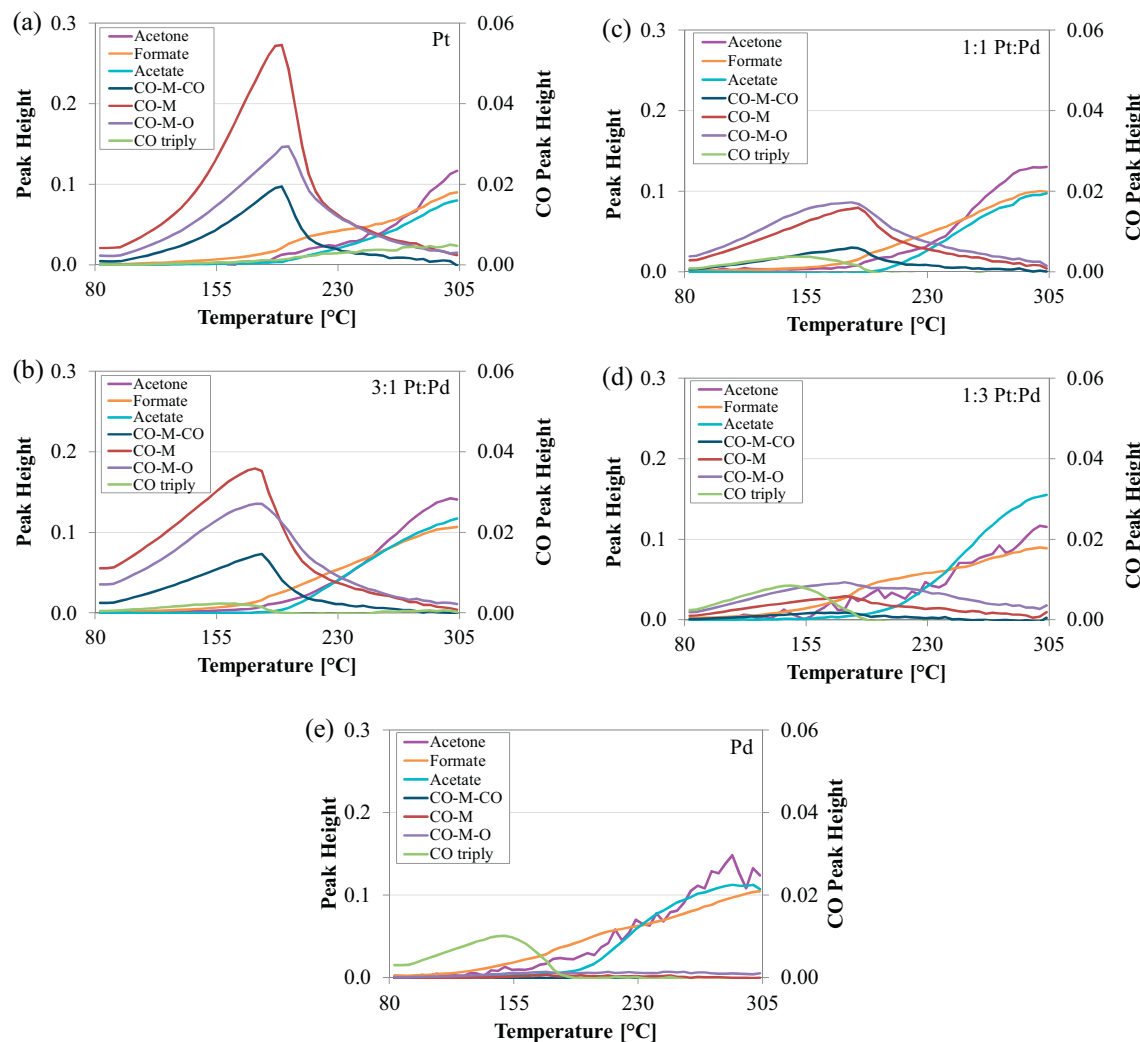


**Fig. 11.** DRIFTS feature peak heights as a function of gas stream temperature for peaks of interest in CO and  $\text{C}_3\text{H}_6$  co-oxidation; acetone [ $1653\text{ cm}^{-1}$ ], formate [ $1600\text{ cm}^{-1}$ ], acetate [ $1450\text{ cm}^{-1}$ ], CO-M-CO [ $2054\text{ cm}^{-1}$ ], CO-M [ $2083\text{ cm}^{-1}$ ], CO-M-O [ $2112\text{ cm}^{-1}$ ], CO triply bound [ $1805\text{ cm}^{-1}$ ]. Feed gas composition: 3000 ppm CO, 1500 ppm  $\text{C}_3\text{H}_6$ , 8%  $\text{O}_2$ , balance He. (a) Pt, (b) 3:1 Pt:Pd, (c) 1:1 Pt:Pd, (d) 1:3 Pt:Pd, (e) Pd.

The CO-M-O peak was observed on both the 3:1 and 1:1 bimetallic catalysts and Pt-only catalyst. The DRIFTS data from the Pd-only catalyst did not contain peaks for any type of single, linearly bound CO at any temperature studied, but instead had a significant triply bound carbonyl peak at low temperatures. For the 1:3 Pt:Pd catalyst, the more significant triply bound carbonyl peak was also observed, in addition to the linear carbonyls associated with the bimetallics. Previous literature [52] has shown that when CO is adsorbed onto bimetallic Pt:Pd particles, neither bridged nor triply bound carbonyls form, but they do on monometallic Pd samples. The presence of both peaks on the 1:3 Pt:Pd catalyst demonstrates both bimetallic and Pd particles were present on the surface, which was also inferred from the EDS results.

Formate and monodentate carbonate surface species formed during CO oxidation on all catalysts. There was no evidence of bicarbonate. This is not meant to conclude that CO oxidation does not occur through a bicarbonate mechanism, it could be that this species reacts too quickly to be observed. The most carbonate formed on the 1:3 and monometallic Pd catalysts, and formation and accumulation of these species could deactivate active sites and result in full conversion not being reached. This was not a monotonic trend, as there was a higher level of both formate and carbonate on the 1:3 Pt:Pd catalyst than on the Pd catalyst, which would suggest if these intermediates inhibited the reaction then

the monometallic Pd sample should have performed better. The 1:3 sample, however, led to a lower CO oxidation light off temperature relative to the monometallic Pd catalyst. This better performance despite the carbonate buildup is attributed to the higher level of CO-M-O, which is apparent on the other more active bimetallic catalysts, suggesting that the alloying promoted formation of highly reactive Pd and Pt oxides. For other Pt-based bimetallic catalysts studied [53] alloying with another metal that easily forms an oxide (Fe, Ni) enabled oxygen dissociation thereby facilitating CO oxidation on Pt, similar to what was observed here. For the 1:1 Pt:Pd catalyst, which performed best in the CO oxidation tests, while there was formate production to a similar extent as on the 1:3 Pt:Pd and Pd catalysts, there was less carbonate formation, and the 1:1 Pt:Pd catalyst was more active than the 1:3 Pt:Pd and Pd catalysts. The Pt and 3:1 Pt:Pd catalysts showed evidence of carbonate formation to a higher extent than the 1:1 Pt:Pd catalyst but not as much as the 1:3 Pt:Pd and Pd catalysts. The data support surface carbonates inhibiting CO oxidation. Similar trends have been observed for Au and CoO<sub>x</sub> catalysts [54,55]. It is not clear whether this carbonate was present on the support or on the metal sites themselves from the spectroscopic results, however it at least seems likely that this species is related to the decreased maximum conversion on the Pd-rich catalysts. The Pd catalyst may simply allow the carbonate to spill over to the support and the decreased conversion was due to

transport effects. And the nonmonotonic trend discussed above is associated with a combination of inhibition by the carbonates and activity of the CO-M-O species. As water is not being introduced as a reactant, formate formation occurred at the edges of the particles bordering Lewis acid sites of alumina [37]. This may be why the carbonate is observed as an inhibitor while the formate is not, as the formate could more easily spill over to the support or play a smaller role at the particle edge.

CO oxidation studied on single Pt atoms [21] suggests a mechanism that goes through a surface carbonate. If the mechanism does go through a carbonate intermediate, then the DRIFTS results suggest that the release of CO<sub>2</sub> through carbonate decomposition in the mechanism may be rate limiting for the 1:3 and Pd samples. For the Pt, 3:1, and 1:1 Pt:Pd catalysts where carbonate did not accumulate to the same extent, the carbonate was either not the primary intermediate in the mechanism or its decomposition to CO<sub>2</sub> is rapid, and thus less was observed. Surface carbonate accumulation leading to a slower ignition rate explains the observed difference in conversion change versus temperature (conversion profile slopes) in the reactor data, its accumulation slows the rate.

To summarize, the lower temperature peak associated with the singly adsorbed carbonyls on the 3:1 Pt:Pd catalyst, Fig. 5 b), is related to carbonyls present on the Pt particles, and the higher temperature peak is attributed to the carbonyl on either the Pt or Pd in a bimetallic particle. This altogether indicates that Pd in a bimetallic particle resulted in an increase in the CO adsorbed on the surface as a co-adsorbed carbonyl with oxygen (CO-M-O), which in turn indicates that the improved light off activity could be related to that available oxygen. Changes in rate of conversion as a function of temperature were also related to surface carbonate decomposition. A trade-off occurs when too much Pd is added, where in addition to the co-adsorbed species there is increased inhibition because of formed carbonate species and eventually the bridge and triple bound sites dominate.

#### 4.3. C<sub>3</sub>H<sub>6</sub> oxidation

For propylene oxidation, the 1:1 and 3:1 Pt:Pd ratios led to the best observed performance. The partial oxidation products produced during propylene oxidation were not sufficient enough to inhibit propylene oxidation to the same extent as over the more Pd-rich samples, and thus the sharper increase in conversion as a function of temperature and no plateau in conversion was observed. In the reactor testing, the 1:1 and 3:1 Pt:Pd catalysts had the least byproduct CO formation and the most acetone formation; while the Pt catalyst resulted in the least ethylene and no acetone formation. The 1:1 and 3:1 Pt:Pd catalysts had the acetone, ethylene, and CO formation all peak at the same temperature just after catalyst light-off. Conversely, byproducts formed over 1:3 and monometallic Pd catalysts did differentiate with temperature; acetone peaked first, ethylene peaked at a slightly higher temperature, and the CO at a higher temperature still. From the DRIFTS results, the CO-M-O peak was the largest on the 1:1 and 3:1 Pt:Pd catalysts during the CO oxidation experiments, while the CO concentrations during propylene oxidation in the reactor testing were the lowest for these catalysts. These catalysts were able to oxidize the byproduct CO relatively easily. The catalysts which were not able to adsorb the CO through the metal oxide, namely the Pd where the CO-M-O peak was not observed during propylene oxidation, had the highest byproduct CO concentrations.

At the beginning of the propylene oxidation experiments, propylidyne was observed in the DRIFTS spectra, giving the strongest absorbance on the 3:1 Pt:Pd catalyst. In previous propylene adsorption and propylene oxidation mechanistic studies on Pt [43,56] this propylene configuration was observed at high propylene coverages, and in the absence of co-adsorbed oxygen [56]. At

low propylene coverages the expected propylene configuration on Pt was di- $\sigma$ -propylene. This suggests that in our study the dehydrogenation of propylene to propylidyne occurred readily at the high propylene concentrations used and that oxygen has limited access to the active sites, leading to only the propylidyne configuration. A previous study [56] has shown 1-methylvinyl species forms via oxydehydrogenation of di- $\sigma$ -propylene. It is this 1-methylvinyl species that has been attributed to the formation of acetone and acetic acid. Formation of acetone is through 1-methylvinyl reacting with oxygen, and acetic acid formation from the removal of the allylic carbon and subsequent oxygen attack on the second carbon. The di- $\sigma$ -propylene or the 1-methylvinyl species were not observed, however acetone was observed both in the DRIFTS spectra and in the reactor testing; this 1-methylvinyl species may be too short lived on the surface to be observed spectroscopically. Since in this study the propylene adsorbed as propylidyne, it is possible that the propylidyne rearranges to 1-methylvinyl leading to the observed acetone formation.

Oxidation to ethylene and CO in various proportions also occurred at light-off. The CO and ethylene formation quantities do not follow a consistent trend with ratio change; which would at first suggest that this is not as simple as the propylene oxidizing to acetone and then the acetone breaking apart directly into only ethylene and CO fragments. From the same study just mentioned [56], under very HC rich conditions the oxygen was entirely consumed in the formation of acetone and little CO<sub>2</sub> formed, while increasing propylene exposure resulted in increased H<sub>2</sub>O and CO production. H<sub>2</sub>O and CO formation implies dehydrogenation of propylidyne and subsequent oxygen attack on the first carbon to form the CO, instead of oxygen attack of the vinyl carbon to form acetone. In other words, when there is not enough oxygen around to form acetone, the formation of ethylene and CO may be preferred. This is supported by our observed results; since the bimetallic catalysts and Pd formed oxides more easily than Pt, the higher surface concentration of oxygen on these catalysts leads to more acetone formation but also subsequent oxygenated hydrocarbon formation. On the Pt catalyst, at higher temperatures oxygen could adsorb and the formation of acetone begin. Since there is not much oxygen on the surface, dehydrogenation reactions occurred leading to preferential ethylene formation. This is supported by the DRIFTS data, where the bimetallic catalysts had the highest peak heights for acetone and acetate develop over the temperature ramp and the Pt catalyst had the smallest acetone features and instead had increased ethylidyne formation. During reactor testing, very low ethylene concentrations were observed with the Pt catalyst, however the DRIFTS results demonstrate that the ethylene remains on the surface. Also in the reactor testing the 1:1 and 3:1 Pt:Pd catalysts yielded the most acetone and acetaldehyde. The 1:1 and 3:1 Pt:Pd catalysts formed roughly equal CO and ethylene concentrations once the catalysts lit off, with the CO and ethylene peaking at the same temperatures, supporting a mechanism where the acetone formation occurs in parallel to propylene oxidizing to ethylene and CO.

For the other Pd-rich catalysts, during reactor testing acetone production peaked at lower temperatures than the ethylene, and ethylene production peaked at lower temperatures than CO, and there was also formation of acetic acid. This may indicate that the dehydrogenation reactions to form the ethylene require a higher activation barrier compared to the oxidation mechanism leading to acetone formation. CO formation over the entire temperature ramp and the fact that full conversion of propylene was not achieved over the 1:3 Pt:Pd and Pd catalysts suggests that the availability of oxygen at the surface was not sufficient for complete oxidation. The DRIFTS results for these catalysts do not suggest the surface was completely taken up by partial oxidation intermediates, as the spectra obtained from the more active 1:1 and 3:1 Pt:Pd catalysts contained larger surface species peak heights. However, during

reactor testing there was higher cumulative partial oxidation product formation with the 1:3 and Pd catalysts over the temperature ramp, especially CO. The formation of these products could lead to inhibition further down the catalyst bed. This would be in combination with the reaction front propagating through the catalyst where local surface concentrations are rapidly changing between a hydrocarbon covered surface to one that has available sites for O<sub>2</sub> dissociation and reaction [22,57].

In general, the bimetallic samples appear to have higher affinity for producing the acetone and acetate species. Acetone is observed on the 1:1 and 3:1 Pt:Pd catalyst surfaces at lower temperatures than the others. For the Pt sample, the CO peak intensity increased at a similar temperature as the 1:1 and 3:1 Pt:Pd catalysts, yet in the reactor testing the onset of propylene oxidation for the Pt catalyst was much later. This suggests that CO being initially formed from propylene partial oxidation strongly inhibited the propylene oxidation onset, especially for Pt as would be expected. Furthermore, the differences in the surface CO and acetone amounts support the notion that propylene oxidation occurs by partial oxidation to CO and ethylene. For the 1:1 and 3:1 Pt:Pd catalysts, the temperatures where CO and acetone started increasing were the same (consistent with trends from bench scale reactor testing); for Pt this was not observed.

Based on the overall results, mechanistic trends across the different Pt:Pd ratios exist. For Pd and 1:3 Pt:Pd, the lower quantity of acetone formed in reactor testing and DRIFTS compared to acetate may indicate that the Pd-rich catalysts either have an easier time breaking the first C–C bond so less C<sub>3</sub> products are formed, or as mentioned before there may be less available surface oxygen. Propylene light-off over the Pd catalyst occurred at a higher temperature compared to the other catalysts tested. The ethylene in the outlet peaks before the CO. The ethylene intermediate on the surface should be easier to oxidize than a methyl group remaining from acetone and acetate formation, which may be the culprit for the larger CO production. Based on the CO oxidation results, it is also possible that carbonate from byproduct CO oxidation could inhibit the reaction and deactivate the catalyst much like what was observed during CO oxidation; except with propylene oxidation there are more partial oxidation intermediates that could form monodentate carbonates and also deactivate the sample. This trend is consistent if we consider the 1:1 and 3:1 Pt:Pd samples; from the CO oxidation experiments such carbonates did not form. Unfortunately, the formation of the monodentate carbonate during propylene oxidation is difficult to monitor due to common peak positions with acetone. Mechanistically, the addition of Pd to a Pt catalyst seems to shift the propylene oxidation mechanism from an indirect dehydrogenation mechanism towards a mechanism directly involving oxygen. Past a certain Pd content, the shift towards the direct oxidation mechanism seems to be detrimental as the required oxygen is not able to adsorb or activate on the surface. The presence of both indirect and direct propylene oxidation mechanisms provides the best performance.

#### 4.4. CO and C<sub>3</sub>H<sub>6</sub> Co-oxidation

In comparing the light off performance ranking under co-oxidation conditions to either CO or propylene oxidation individually, the trend in the ranking more closely resembles that for CO oxidation. This was expected due to strong CO poisoning/adsorption. For instance, in comparing the monometallic Pt sample results, CO oxidation light off occurred at a higher temperature than that of the other samples, as is also the case for the CO and propylene co-oxidation, whereas the Pt sample was not the worst performing for propylene oxidation. The relative amounts of the CO–M–O to CO–M differ between CO oxidation and CO and propylene co-oxidation. During co-oxidation, there

was a decreased amount of the CO–M–O and more CO–M and CO–M–CO, compared to the amounts observed during CO oxidation by itself. Since the CO–M–O was associated with high CO oxidation activity, and there was less, lower reactivity would be expected and was indeed observed with the addition of propylene. Since more CO–M and CO–M–CO are observed, this suggests there is less surface O available for formation of CO–M–O, suggesting that propylene inhibited CO oxidation by blocking the oxygen from accessing the active sites via competitive adsorption. Note, the position of the CO–M–O peak also corresponds to that for CO–M–CO, and in this co-oxidation case the CO–M–CO peaks are not trivial. Therefore, the assignment cannot be solely attributed to CO–M–O species but also to CO–M–CO species. This only further highlights the lack of oxygen availability alluded to in the previous discussion. Furthermore, from the DRIFTS peak height as a function of temperature results for co-oxidation, the peak height maximum for the various CO species occurred at a much lower temperature than for CO oxidation alone. This occurred at the same time as formate formation and at slightly higher temperatures the acetone and acetate peak heights increased. Thus some CO is oxidizing through a formate intermediate and making room for propylene adsorption and oxidation to the partial oxidation surface species. This is evidence of competitive adsorption that is leading to the inhibition of both CO and propylene during co-oxidation.

The above comparisons help mechanistically explain how propylene inhibits CO oxidation, and can also describe why there are different rates of conversion change versus temperature. As the Pd content increased, the direct oxidation mechanism became favored, which led to a larger amount of poisoning by inhibiting surface species, consistent with what was observed during propylene oxidation discussed earlier. Similar byproducts were observed during reactor testing, but were lower in comparison to propylene oxidation in the absence of CO. Propylene oxidation is inhibited until the CO desorbs or is oxidized, and therefore lower partial oxidation species concentrations were ultimately observed because the catalyst was at a higher temperature when they form, and was able to more easily oxidize them as they formed. If the direct oxidation mechanism for propylene was indeed the dominant mechanism for the Pd-rich catalysts, this would be consistent with the large offset between the CO and propylene conversion profile and the lower overall conversion for the 1:3 Pt:Pd catalyst seen in co-oxidation compared to oxidation of each component individually. Since there was less available surface oxygen with propylene present due to competitive adsorption, and the direct oxidation mechanism was favored compared to indirect oxidation, more inhibition of the Pd-rich catalyst was observed.

## 5. Conclusions

CO and propylene oxidation, in high reactant concentrations, was studied over Pt–Pd bimetallic catalysts with different Pt:Pd ratios. In evaluating CO oxidation, bimetallic catalysts with a higher Pd content led to lower temperature CO oxidation activity, and this was related to how the CO bound to the bimetallic surface. CO–M–O species, M being the metal, were observed during DRIFTS experiments and were correlated to the most active bimetallic samples. In contrast to the bimetallic samples, CO–M–CO species were observed on the monometallic Pt sample before light off, further demonstrating the greater sensitivity Pt has to CO poisoning. Indeed, with increasing CO concentration, the Pt catalyst was the most affected in terms of increasing inhibition. The Pd-rich catalysts, i.e. the 1:3 Pt:Pd and monometallic Pd samples, appear to be inhibited, or deactivated, through surface carbonate formation. For propylene oxidation, the shift in the T<sub>50</sub> with increased concentration did not depend on the Pt:Pd ratio; however, there was

evidence of partial oxidation product inhibition, due to at least acetone, ethylene, and CO, all observed as surface species/byproducts. The increased rate at which these partial oxidation species accumulate on Pd-rich catalysts coincide with the poorer performance observed during reaction tests. A shift between indirect oxidation on Pt towards direct oxidation on Pd being favored as a function of Pt:Pd ratio was discussed and supported by the observed reaction intermediates. For the 1:1 and 3:1 Pt:Pd catalysts, both mechanisms seem to occur in parallel and a higher surface oxygen availability led to a low temperature light off. For the Pt catalyst, the dehydrogenation mechanism is favored. The available surface oxygen is limiting for both the Pd and Pt catalysts.

In comparison to the single component CO and propylene oxidation, catalyst performance trends during co-oxidation of the two species, indicated by  $T_{50}$ , mirror those of CO oxidation by itself. With propylene present in the gas feed, the CO–M–O species was less favored; more triply bound, single carbonyl, and dicarbonyl species were evident. The greater inhibition observed on the monometallic Pt sample was attributed to the greater amount of CO–M–CO species formed, much like in the evaluation of CO oxidation in the absence of propylene. The greater deactivation of the Pd-rich catalyst was attributed to partial oxidation species formation; in this case suffering from both carbonate formation from CO oxidation, as well as partial oxidation products formation from propylene oxidation. The data also indicate that propylene inhibits oxygen availability to the active sites and therefore inhibited CO oxidation light off.

## Acknowledgement

We thank the US Department of Energy and the National Science Foundation (CBET 1258688) for financial support.

## Appendix A. Supplementary data

Supplementary data associated with this article can be found, in the online version, at <http://dx.doi.org/10.1016/j.apcatb.2016.09.034>.

## References

- V.Y. Prihodko, S.J. Curran, T.L. Barone, S.A. Lewis, J.M. Storey, K. Cho, et al., Diesel oxidation catalyst control of hydrocarbon aerosols from reactivity controlled compression ignition combustion, *Am. Soc. Mech. Eng. Int. Mech. Eng. Conf. Expo.* (2011) 273–278, <http://dx.doi.org/10.1115/IMECE2011-64147>.
- V.Y. Prihodko, S.J. Curran, J.E. Parks, R.M. Wagner, Effectiveness of diesel oxidation catalyst in reducing HC and CO emissions from reactivity controlled compression ignition, *SAE Int. J. Fuels Lubr.* 6 (2013) 329–335, <http://dx.doi.org/10.4271/2013-01-0515>.
- J.C. Summers, L.L. Hegedus, Effects of platinum and palladium impregnation on the performance and durability of automobile exhaust oxidizing catalysts, *J. Catal.* 51 (1978) 185–192, [http://dx.doi.org/10.1016/0021-9517\(78\)90292-0](http://dx.doi.org/10.1016/0021-9517(78)90292-0).
- M. Kaneeda, H. Iizuka, T. Hiratsuka, N. Shinotsuka, M. Arai, Improvement of thermal stability of NO oxidation Pt/Al2O3 catalyst by addition of Pd, *Appl. Catal. B Environ.* 90 (2009) 564–569, <http://dx.doi.org/10.1016/j.apcatb.2009.04.011>.
- M. Chen, L.D. Schmidt, Morphology and composition of Pt-Pd alloy crystallites on SiO<sub>2</sub> in reactive atmospheres, *J. Catal.* 56 (1979) 198–218.
- A. Morlang, U. Neuhausen, K.V. Klementiev, F.-W. Schütze, G. Miehe, H. Fuess, et al., Bimetallic Pt/Pd diesel oxidation catalysts, *Appl. Catal. B Environ.* 60 (2005) 191–199, <http://dx.doi.org/10.1016/j.apcatb.2005.03.007>.
- R. Chen, Z. Chen, B. Ma, X. Hao, N. Kapur, J. Hyun, et al., CO adsorption on Pt (111) and Pd (111) surfaces: a first-principles based lattice gas Monte-Carlo study, *Comput. Theor. Chem.* 987 (2012) 77–83, <http://dx.doi.org/10.1016/j.comptc.2011.07.015>.
- M. Skoglundh, L.O. Löwendahl, J. Otterstedt, Combinations of platinum and palladium on alumina supports as oxidation catalysts, *Appl. Catal.* 77 (1991) 9–20, [http://dx.doi.org/10.1016/0166-9834\(91\)80019-S](http://dx.doi.org/10.1016/0166-9834(91)80019-S).
- B.M. Shakya, B. Sukumar, Y.M. López-De Jesús, P. Markatou, The effect of Pt:Pd ratio on heavy-Duty diesel oxidation catalyst performance: an experimental and modeling study, *SAE Int. J. Engines* 8 (2015) 1271–1282, <http://dx.doi.org/10.4271/2015-01-1052>.
- T. Rades, C. Pak, M. Polisset-Thfoin, R. Ryoo, J. Fraissard, Characterization of bimetallic naY-supported Pt-Pd catalyst by EXAFS, TEM and TPR, *Catal. Lett.* 29 (1994) 91–103, <http://dx.doi.org/10.1007/BF00814255>.
- T. Rades, V.Y. Borovkov, V.B. Kazansky, M. Polisset-Thfoin, J. Fraissard, Diffuse reflectance IR study of CO adsorption on a bimetallic Pt – Pd catalyst supported on NaY zeolite. evidence of alloy formation, *J. Phys. Chem. Ref. Data* 40 (1996) 16238–16241, <http://dx.doi.org/10.1021/jp9606063>.
- Y. Yu, B. Fonfè, A. Jentys, G.L. Haller, J.a.R. van Veen, O.Y. Gutiérrez, et al., Bimetallic Pt-Pd/silica-alumina hydrotreating catalysts –Part I: physicochemical characterization, *J. Catal.* 292 (2012) 1–12, <http://dx.doi.org/10.1016/j.jcat.2012.03.017>.
- P.L. Hansen, A.M. Molenbroek, A.V. Ruban, Alloy formation and surface segregation in zeolite-Supported Pt-Pd bimetallic catalysts, *J. Phys. Chem. B* 101 (1997) 1861–1868, <http://dx.doi.org/10.1021/jp9627710>.
- T. Fujikawa, K. Tsuji, H. Mizuguchi, H. Godo, K. Idei, K. Usui, EXAFS characterization of bimetallic Pt – Pd/SiO<sub>2</sub> – Al 2 O 3 catalysts for hydrogenation of aromatics in diesel fuel, *Catal. Lett.* 63 (1999) 27–33, <http://dx.doi.org/10.1023/A:1019008803028>.
- J. Roussel, A.J. Renouprez, A.M. Cadrot, Ion-scattering study and Monte Carlo simulations of surface segregation in Pd-Pt nanoclusters obtained by laser vaporization of bulk alloys, *Phys. Rev. B* 58 (1998) 2150–2156, <http://dx.doi.org/10.1103/PhysRevB.58.2150>.
- L.C.A. van den Oetelaar, O.W. Nooij, S. Oerlemans, A.W. Denier Van Der Gon, H.H. Brongersma, Surface segregation in supported Pd-Pt nanoclusters and alloys, *J. Phys. Chem. B* 102 (1998) 3445–3455.
- T.R. Johns, J.R. Gaudet, E.J. Peterson, J.T. Miller, E.A. Stach, C.H. Kim, et al., Microstructure of bimetallic Pt-Pd catalysts under oxidizing conditions, *ChemCatChem* 5 (2013) 2636–2645, <http://dx.doi.org/10.1002/cctc.201300181>.
- K. Zorn, S. Giorgio, E. Halwax, C.R. Henry, H. Grönbeck, G. Rupprechter, CO oxidation on technological Pd – Al 2 O 3 catalysts: oxidation state and activity, *J. Phys. Chem. C* 115 (2011) 1103–1111, <http://dx.doi.org/10.1021/jp106235x>.
- C. Karakaya, O. Deutschmann, A simple method for CO chemisorption studies under continuous flow: adsorption and desorption behavior of Pt/Al2O3 catalysts, *Appl. Catal. A Gen.* 445–446 (2012) 221–230, <http://dx.doi.org/10.1016/j.apcata.2012.08.022>.
- J.R. Anderson, *Structure of Metallic Catalysts*, Academic Press, London, 1975.
- M. Moses-Debusk, M. Yoon, L.F. Allard, D.R. Mullins, Z. Wu, X. Yang, et al., CO oxidation on supported single Pt atoms: experimental and ab initio density functional studies of CO interaction with Pt atom on  $\theta$ -Al 2O3(010) surface, *J. Am. Chem. Soc.* 135 (2013) 12634–12645, <http://dx.doi.org/10.1021/ja401847c>.
- M.J. Hazlett, W.S. Epling, Spatially resolving CO and C3H6 oxidation reactions in a Pt/Al2O3 model oxidation catalyst, *Catal. Today* 267 (2016) 157–166, <http://dx.doi.org/10.1016/j.cattod.2015.11.033>.
- G. Busca, E. Finocchio, V.S. Escrivano, Infrared studies of CO oxidation by oxygen and by water over Pt/Al2O3 and Pd/Al2O3 catalysts, *Appl. Catal. B Environ.* 113–114 (2012) 172–179, <http://dx.doi.org/10.1016/j.apcatb.2011.11.035>.
- C.M. Grill, R.D. Gonzalez, Infrared study of the adsorption of CO and NO on silica-Supported pd and Pt-Pd, *J. Phys. Chem.* 84 (1980) 878–882, <http://dx.doi.org/10.1021/j100445a018>.
- J.T. Yates, T.M. Duncan, S.D. Worley, R.W. Vaughan, Infrared spectra of chemisorbed CO on Rh, *J. Chem. Phys.* 70 (1979) 1219–1224, <http://dx.doi.org/10.1063/1.437603>.
- J.G. Goodwin, C. Naccache, CO adsorption on ion-exchanged Ru zeolite catalyst, *J. Catal.* 64 (1980) 482–486, [http://dx.doi.org/10.1016/0021-9517\(80\)90520-5](http://dx.doi.org/10.1016/0021-9517(80)90520-5).
- E.V. Benvenutti, L. Franken, C.C. Moro, FTIR study of hydrogen and carbon monoxide adsorption on Pt/TiO<sub>2</sub>, Pt/ZrO<sub>2</sub>, and Pt/Al 2 O 3, *Langmuir* 15 (1999) 8140–8146, <http://dx.doi.org/10.1021/la990195s>.
- M.A. Vannice, C.C. Twu, S.H. Moon, SMSI effects on CO adsorption and hydrogenation on Pt catalysts – I. Infrared spectra of adsorbed CO prior to and during reaction conditions, *J. Catal.* 79 (1983) 70–80, [http://dx.doi.org/10.1016/0021-9517\(83\)90290-7](http://dx.doi.org/10.1016/0021-9517(83)90290-7).
- M. Primet, Electronic transfer and ligand effects in the infrared spectra of adsorbed carbon monoxide, *J. Catal.* 88 (1984) 273–282, [http://dx.doi.org/10.1016/0021-9517\(84\)90003-4](http://dx.doi.org/10.1016/0021-9517(84)90003-4).
- M. Primet, J.M. Basset, M.V. Mathieu, M. Prettre, Infrared Study of CO Adsorbed on Pt/Al2O3. A method for determining metal-adsorbate interactions, *J. Catal.* 29 (1973) 213–223, [http://dx.doi.org/10.1016/0021-9517\(73\)90225-X](http://dx.doi.org/10.1016/0021-9517(73)90225-X).
- H. Heyne, F.C. Tompkins, Application of infrared spectroscopy and surface potential measurements in a study of the oxidation of carbon monoxide on platinum, *Proc. R. Soc. A* 292 (1966) 460–478, <http://dx.doi.org/10.1098/rspa.1963.0054>.
- G. Busca, J. Lamotte, J.-C. Lavalle, V. Lorenzelli, FT-IR study of the adsorption and transformation of formaldehyde on oxide surfaces, *J. Am. Chem. Soc.* 109 (1987) 5197–5202.
- M.I. Zaki, M.A. Hasan, L. Pasupulety, Surface reactions of acetone on Al2O3, TiO<sub>2</sub>, ZrO<sub>2</sub>, and CeO<sub>2</sub>: IR spectroscopic assessment of impacts of the surface acid – base properties, *Langmuir* 17 (2001) 768–774.
- A.A. Davydov, *Infrared Spectroscopy of Adsorbed Species on the Surfaces of Transition Metal Oxides*, John Wiley & Sons, Chichester, 1990.

[35] Y. Zhu, H. Uchida, M. Watanabe, Oxidation of carbon monoxide at a platinum film electrode studied by fourier transform infrared spectroscopy with attenuated total reflection technique, *Langmuir* 15 (1999) 8757–8764.

[36] K.I. Hadjiiivanov, G.N. Vayssilov, Characterization of oxide surfaces and zeolites by carbon monoxide as an IR probe molecule, *Adv. Catal.* 47 (2002) 307–511, [http://dx.doi.org/10.1016/S0360-0564\(02\)47008-3](http://dx.doi.org/10.1016/S0360-0564(02)47008-3).

[37] M.M. Schubert, H.A. Gasteiger, R. Jürgen Behm, Surface formates as side products in the selective CO oxidation on Pt/γ-Al<sub>2</sub>O<sub>3</sub>, *J. Catal.* 172 (1997) 256–258.

[38] C. Daniel, M.-O. Clarté, S.P. Teh, O. Thimon, H. Provendier, A.C. Van Veen, et al., Spatially resolved catalysis in microstructured reactors by IR spectroscopy: CO oxidation over mono- and bifunctional Pt catalysts, *J. Catal.* 272 (2010) 55–64, <http://dx.doi.org/10.1016/j.jcat.2010.03.012>.

[39] J.L. Robbins, E. Maruccchi-Soos, Evidence for multiple CO hydrogenation pathways on Pt/Al<sub>2</sub>O<sub>3</sub>, *Am. Chem. Soc.* 2885 (1989) 2885–2888.

[40] T. Iwasita, F.C. Nart, Identification of methanol adsorbs on platinum: an *in situ* FT-IR investigation, *Electroanal. Chem.* 317 (1991) 291–298.

[41] N. Cant, W.K. Hall, Catalytic oxidation II. Silica supported noble metals for the oxidation of ethylene and propylene, *J. Catal.* 16 (1970) 220–231, [http://dx.doi.org/10.1016/0021-9517\(70\)90216-2](http://dx.doi.org/10.1016/0021-9517(70)90216-2).

[42] N. Cant, W. Hall, Catalytic oxidation. IV. Ethylene and propylene oxidation over gold, *J. Phys. Chem.* 76 (1971) 2914–2921, <http://dx.doi.org/10.1021/j100688a007>.

[43] F. Zaera, D. Chrysostomou, Propylene on Pt (111) I. Characterization of surface species by infra-red spectroscopy, *Surf. Sci.* 457 (2000) 71–88, [http://dx.doi.org/10.1016/S0039-6028\(00\)00337-X](http://dx.doi.org/10.1016/S0039-6028(00)00337-X).

[44] A.A. Davydov, V.G. Mikhaltchenko, V.D. Sokolovskii, Surface complexes of propylene and their role in catalytic oxidation, *J. Catal.* 55 (1978) 299–313, [http://dx.doi.org/10.1016/0021-9517\(78\)90218-X](http://dx.doi.org/10.1016/0021-9517(78)90218-X).

[45] J. Datka, Z. Sarbak, R.P. Eischens, Infrared study of coke on alumina and zeolite, *J. Catal.* 145 (1994) 544–550.

[46] K. Shimizu, H. Kawabata, A. Satsuma, T. Hattori, Role of acetate and nitrates in the selective catalytic reduction of NO by propene over alumina catalyst as investigated by FTIR, *J. Phys. Chem. B.* 103 (1999) 5240–5245, <http://dx.doi.org/10.1021/jp984770x>.

[47] M.A. Vannice, W. Erley, H. Ibach, A RAIRS and HREELS study of acetone on Pt(111), *Surf. Sci.* 254 (1991) 1–11.

[48] J.C. De Jesús, F. Zaera, Adsorption and thermal chemistry of acrolein and crotonaldehyde on Pt(111) surfaces, *Surf. Sci.* 430 (1999) 99–115, [http://dx.doi.org/10.1016/S0039-6028\(99\)00406-9](http://dx.doi.org/10.1016/S0039-6028(99)00406-9).

[49] S.B. Mohsin, M. Trenary, Infrared identification of the low-temperature forms of ethylene adsorbed on Pt/Al<sub>2</sub>O<sub>3</sub>, *J. Phys. Chem.* 92 (1998) 5229–5233.

[50] J. Raskó, T. Kecskés, J. Kiss, Formaldehyde formation in the interaction of HCOOH with Pt supported on TiO<sub>2</sub>, *J. Catal.* 224 (2004) 261–268, <http://dx.doi.org/10.1016/j.jcat.2004.03.025>.

[51] C.M. Grill, M.L. McLaughlin, J.M. Stevenson, D. Richard, Characterization of supported using infrared spectroscopy bimetallic clusters, *J. Catal.* 69 (1981) 454–464.

[52] R.D. Gonzalez, C. Grill, Infrared evidence for the segregation of silica-supported Pt-Pd bimetallic clusters in oxidizing atmospheres, *J. Catal.* 64 (1980) 487–490, [http://dx.doi.org/10.1016/0021-9517\(80\)90521-7](http://dx.doi.org/10.1016/0021-9517(80)90521-7).

[53] W. Yu, M.D. Porosoff, J.G. Chen, Review of Pt-based bimetallic catalysis: from model surfaces to supported catalysts, *Chem. Rev.* 112 (2012) 5780–5817, <http://dx.doi.org/10.1021/cr300096b>.

[54] P. Thormählen, M. Skoglundh, E. Fridell, B. Andersson, Low-temperature CO oxidation over platinum and cobalt oxide catalysts, *J. Catal.* 188 (1999) 300–310, <http://dx.doi.org/10.1006/jcat.1999.2665>.

[55] R. Burch, Gold catalysts for pure hydrogen production in the water-gas shift reaction: activity, structure and reaction mechanism, *Phys. Chem. Chem. Phys.* 8 (2006) 5483–5500, <http://dx.doi.org/10.1039/b607837k>.

[56] A.M. Gabelnick, Catalytic oxidation of C<sub>3</sub> hydrocarbons: *in situ* mechanistic studies on platinum and supported platinum surfaces, in: Dissertation (Doctoral thesis), Department of Chemistry, University of Michigan, 2000.

[57] A. Russell, W.S. Epling, Diesel oxidation catalysts, *Catal. Rev.* 53 (2011) 337–423.